AGU PUBLICATIONS

JGR

Journal of Geophysical Research: Atmospheres

RESEARCH ARTICLE

10.1002/2013JD020827

Key Points:
- CCN activity of aerosol particles with different hygroscopicity was investigated
- Measured and predicted CCN activation diameters were compared
- Less hygroscopic particles contributed substantially to cloud droplet formation

Supporting Information:
- Readme
- Figures S1–S8

Correspondence to:
M. Mochida,
mochida.michihiro@g.mbox.nagoya-u.ac.jp

Citation:
Kawana, K., N. Kuba, and M. Mochida (2014), Assessment of cloud condensation nucleus activation of urban aerosol particles with different hygroscopicity and the application to the cloud parcel model, *J. Geophys. Res. Atmos.*, *119*, 3352–3371, doi:10.1002/2013JD020827.

Received 5 SEP 2013
Accepted 17 FEB 2014
Accepted article online 24 FEB 2014
Published online 27 MAR 2014

Assessment of cloud condensation nucleus activation of urban aerosol particles with different hygroscopicity and the application to the cloud parcel model

Kaori Kawana[1], Naomi Kuba[2,3], and Michihiro Mochida[1]

[1]Graduate School of Environmental Studies, Nagoya University, Nagoya, Japan, [2]Research Institute for Global Change, Japan Agency for Marine-Earth Science and Technology, Yokohama, Japan, [3]Also at Atmosphere and Ocean Research Institute, University of Tokyo, Kashiwa, Japan

Abstract Size-resolved measurements of the ratios of cloud condensation nuclei (CCN) to condensation nuclei for particles with different hygroscopic growth factors (g) and distributions of g at 85% relative humidity were performed for urban aerosols over Nagoya, Japan. The CCN efficiency spectra of less hygroscopic particles (g of 1.0 and 1.1) were very different from those of more hygroscopic particles (g of 1.25 and 1.4). While the differences between the CCN activation diameters predicted from g ($d_{act,g85}$) and those measured ($d_{act,CCN}$) were within 12% for more hygroscopic particles, the differences were larger (16%–41%) for less hygroscopic particles. Possible causes of this included surface tension reduction, the dependence of κ on the concentration of the solution, the existence of sparingly soluble materials, and asphericity of particles. The number concentrations of CCN (N_{CCN}) and cloud droplets (N_{cd}) and the effective radius of cloud droplets (R_{eff}) were estimated from the distributions of g using a cloud parcel model. The influences of the differences between $d_{act,g85}$ and $d_{act,CCN}$ and the existence of CCN-inactive particles on the model assessment were small. With high updraft velocity, incorporating both less and more hygroscopic particles into the model led to substantial increases in N_{CCN} and N_{cd} and a decrease in R_{eff} as compared to the hypothetical cases that only more hygroscopic particles were present. The results indicated that less hygroscopic particles significantly contribute to cloud droplet formation and assessments of g distributions are useful in this regard.

1. Introduction

Aerosol particles in the atmosphere affect global climate change directly by absorbing and scattering solar radiation, and indirectly by acting as cloud condensation nuclei (CCN). According to the Fourth Assessment Report of the *Intergovernmental Panel on Climate Change* [2007], the radiative forcing from indirect effects, because of the influence of aerosols on clouds, has large uncertainty, and the assessment of current and future climate change remains a challenge. The increases of CCN(N_{CCN}) and cloud droplet number concentrations (N_{cd}) and the decrease of cloud droplet effective radius (R_{eff}) lead to the increase of cloud albedo and the cooling of the atmosphere, the so-called first indirect effect [*Twomey*, 1977]. Further, they lead to prolonged cloud lifetime and precipitation reduction, the so-called second indirect effect [*Albrecht*, 1989]. Some satellite observations have indicated that cloud droplets in clouds affected by the smoke of biomass burning and anthropogenic activity did not grow even at high altitude and that precipitation was suppressed as compared to smoke- or plume-free clouds [*Rosenfeld*, 1999, 2000]. Some model calculations have also indicated that the increase of the proportion of anthropogenic aerosols leads to changes in surface air temperature and precipitation [*Menon et al.*, 2002; *Takemura et al.*, 2005]. Moreover, in-cloud processes change the composition, properties, and formation and loss of aerosols. For example, the formation of sulfate and organic acids may occur in clouds [*Ervens et al.*, 2004a; *Wonaschuetz et al.*, 2012] and the size distributions of aerosols may change through cloud cycles [*Ervens et al.*, 2004b]. Wet deposition is an important mechanism of atmospheric aerosols and controls the residence time and concentrations.

CCN activation of aerosol particles are investigated based on the theoretical activation curve proposed by Köhler, which considers both the Kelvin effect (the increase of the equilibrium water vapor pressure resulting from the curved liquid-vapor interface) and the Raoult effect (the decrease of the equilibrium water vapor pressure by the presence of solute). Many studies have focused on the relationship between hygroscopicity under subsaturated conditions and the CCN activity under supersaturated conditions. In field studies, the ability

of aerosol particles to form cloud droplets have been investigated using a hygroscopicity tandem differential mobility analyzer (HTDMA) and a CCN counter (CCNC). In these studies, the hygroscopicity of particles was measured using HTDMA, and the CCN number concentration (N_{CCN}) was predicted based on the measured hygroscopicity and the number-size distributions of particles [*Rissler et al*., 2004; *Vestin et al*., 2007; *Fors et al*., 2011]. N_{CCN} predicted from the HTDMA data and those calculated/measured from the CCNC data agreed in some cases [*Mochida et al*., 2011] but were also found to disagree [*Gasparini et al*., 2006], and the disparity may be the result of air mass origins and atmospheric environments. Controversial results have also been reported for laboratory-generated secondary organic aerosol (SOA) particles; the critical supersaturation (S_{crit}) calculated from HTDMA and CCNC data in some cases agreed [*Duplissy et al*., 2008] but in other cases did not [*Prenni et al*., 2007; *Good et al*., 2010]. Many possible causes for this discrepancy have been proposed, including reduced surface tension due to surface-active compounds, presence of solid core or low-solubility components, low accommodation coefficient of water by the film-forming compounds, bulk to surface partitioning, change of water activity (a_w) coefficient with dilution, and asphericity of particles [*Shulman et al*., 1996; *Chuang*, 2003; *Shantz et al*., 2003; *Bilde and Svenningsson*, 2004; *Broekhuizen et al*., 2004; *Abbatt et al*., 2005; *Henning et al*., 2005; *Sjogren et al*., 2007; *Wex et al*., 2009; *Tritscher et al*., 2011]. However, the extent and causes of the discrepancies under different atmospheric conditions and in different laboratory studies remain open questions.

At a large scale, aerosol-cloud interaction has been the subject of many modeling studies. These studies have investigated the influences of aerosol physical properties (number concentration and size distribution), chemical properties (chemical composition and hygroscopicity), and the above mentioned effects of organics on cloud properties (cloud droplet number concentration and indirect radiative forcing). Some studies have shown that the influences of chemical properties of aerosol particles and the effects of organics on the cloud activation are particularly significant in polluted environments [*Lance et al*., 2004; *Leaitch et al*., 2010]. In contrast, other studies have shown that the effects of aerosol physical properties are important and that the effects of chemical properties and organics are small [*Fountoukis et al*., 2007; *Reutter et al*., 2009]. *Anttila et al*. [2009] calculated the activated fractions of particles from HTDMA-derived hygroscopic growth factors (g) at ~90% relative humidity (RH) and considering the size distributions of cloud droplets during cloud events; they reported that the slight changes of the fit-based mean g, to 0.95 or 1.05 times and to 0.9 or 1.1 times the original values, resulted in changes in the soluble volume fractions (16%–33%) and N_{cd} (10%–50%). *Liu and Wang* [2010] calculated that changing κ of primary organic aerosol (POA) from 0 to 0.1 and κ of SOA from 0.14 to 0.07 or 0.21 (±50%) resulted in a 40%–80% increase and ≤40% change, respectively, of the global average N_{CCN} at 0.1% supersaturation (SS). These results indicated that the hygroscopicity of aerosol particles had a large impact on particle activation. However, few studies have quantitatively investigated the influences and contributions of aerosol properties on cloud properties based on detailed hygroscopicity data, such as the distributions of g and CCN activity.

Here, we present an urban aerosol study that used HTDMA and the information on the aerosol mixing state that could be obtained from g [*Cubison et al*., 2008; *Wang et al*., 2010]. In this study, the relationship between hygroscopicity and CCN activity of aerosol particles was investigated based on the observation of atmospheric aerosol particles using the HTDMA and CCNC in Nagoya, Japan, in July and August 2010. The ratios of CCN to condensation nuclei (CN) for aerosol particles with different g of 1.0, 1.1, 1.25, and 1.4 at 16 dry mobility diameters ($d_{p,dry}$) were measured as a novel method to assess the CCN activity of particles with known hygroscopicity. In addition, the number-size distributions and the distributions of g at 85% RH were measured. For particles with different g, the characteristics of CCN activation were examined based on CCN efficiency spectra. Further, the relationship between the particle hygroscopic growth under subsaturated conditions and the CCN activity under supersaturated conditions was investigated by comparing CCN activation diameters predicted from g ($d_{act,g85}$) versus measured values ($d_{act,CCN}$). The data were then utilized to investigate the contribution of particles with different hygroscopicity to cloud droplet formation using a cloud parcel model. The performance of the model was interpreted in view of the influences of the differences between $d_{act,g85}$ and $d_{act,CCN}$ and the presence of CCN-inactive particles. Further, N_{CCN}, N_{cd}, and R_{eff} were estimated considering particles with different ranges of g.

2. Methods

2.1. Aerosol Measurements

Aerosol observations were made at Higashiyama campus, Nagoya University (35°09′N, 136°58′E) in the city of Nagoya, Japan, from 29 July to 3 August 2010. The schematic of the instruments is shown in Figure 1. The inlet

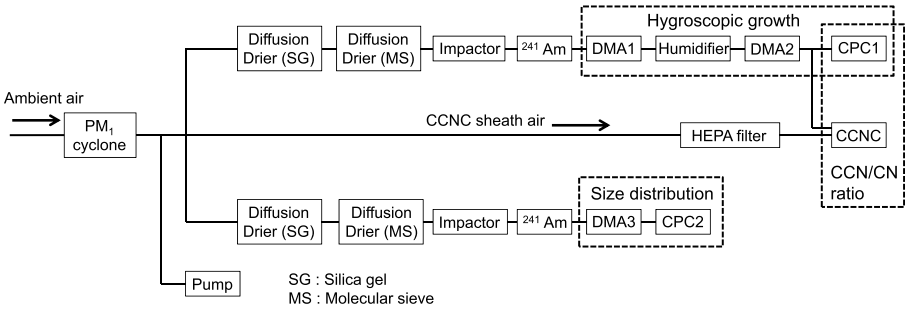

Figure 1. Schematic of the instruments.

was placed at 9.5 m above ground level (AGL). Aerosol particles were introduced into a PM_1 cyclone (URG) at a flow rate of 16.7 L min^{-1}. After the removal of coarse mode particles, aerosols were dried (RH $<$ 2%) in two diffusion driers, one filled with silica gel and the other with a molecular sieve (13X/4A mixture, Spelco, and Sigma-Aldrich). The particles were passed through the impactor and the neutralizer, and those having $d_{p,dry}$ from 24.1 to 359 nm were separated in the first DMA (DMA1; Model 3081, TSI Inc.) of the HTDMA. After humidification in Nafion tubing (MD110-24S-4, Perma Pure LLC), the particles were further separated in the second DMA (DMA2, Models 3080, and 3081, TSI Inc.) at 85 ± 1% RH (at the exit of the DMA column, with consideration of the accuracy of the sensors) to select particles with specific g (g_{set}) around 1.0, 1.1, 1.25, and 1.4. The particles with the selected $d_{p,dry}$ and g_{set} were introduced to the CCN counter (CCNC, Droplet Measurement Technologies) and the condensation particle counter (CPC1, Model 3775, TSI Inc.). The number concentrations of CCN ($n_{DMA2,CCN}$) and CN ($n_{DMA2,CN}$) for particles with g_{set} of 1.0, 1.1, 1.25, and 1.4 were measured by the CCNC and CPC1, respectively, under supersaturation (SS) conditions of 0.18%, 0.49%, and 0.95%. Measurements were performed 4 times for particles with g_{set} of 1.0, 1.1, 1.25, and 1.4 at 0.18%, 0.49%, and 0.95% SS. The g distributions were obtained for 16 sizes, from 24.1 to 359 nm, for particles in the range of $0.8 \le g \le 2.2$ as averages of the results from two measurements during 0600−0900 LT and those during 1800−2100 LT. Measurements were performed for 11 time periods during the observation. Temperature and humidity in the HTDMA were monitored using sensors (HMT 337, Vaisala). We verified that the sample flow exiting DMA1 (upstream of the humidifier) was dried (RH $<$ 2%) and that the sample and sheath flows entering DMA2 and the sheath flow exiting DMA2 were humidified (~85% RH). The mean particle residence time in the sample line downstream of the humidifier and upstream of DMA2, where RH was expected to be stabilized to ~85% was estimated to be 12 s. The sample flow rates of the DMAs in the HTDMA were 0.35 L min^{-1}. The ratios of the sheath to sample flow rates for the DMAs were 10:1.

A portion of the sample aerosols that passed through the PM_1 cyclone was subjected to number-size distribution measurements using a scanning mobility particle sizer (SMPS). The SMPS is composed of a DMA (DMA3, Models 3080, and 3081, TSI Incorporated) with a temperature and humidity sensor at the exit of the sheath line (HMT 337, Vaisala) and a CPC (CPC2; Model 3025A, TSI Incorporated). The size distributions from 14.1 to 711 nm were measured every 5 min. The sheath flow exiting DMA3 was confirmed to be dried (RH $<$ 5%) during the observation. The sample flow rate of the SMPS was 0.3 L min^{-1}. The ratio of the sheath to sample flow rate was 10:1.

2.2. Calibration and Data Processing

Standard polystyrene latex (PSL) spheres (STADEX, JSR Corporation; mean diameter ± the expanded uncertainty (CV): 48 ± 1 nm (15.57%), 100 ± 3 nm (2.47%), 309 ± 9 nm (1.13%)) were introduced to the three DMAs in the HTDMA and the SMPS to examine instrument performance prior to making field measurements. The mode diameters of the normal functions fitted to the measured number-size concentrations for 100 nm and 309 nm PSL spheres, with the consideration of the width of the DMA transfer function, were on average within the range of mean diameter ± the expanded uncertainty described above, while those of the 48 nm PSL spheres were 1 nm off from the range described above. Ammonium sulfate particles (99.999% purity, Sigma-Aldrich) were introduced to the CCNC to calibrate the SS conditions before and after atmospheric observation. The CCN efficiency spectra of singly charged particles were obtained with consideration of the presence of multiply charged particles. The influences of the presence of multiply charged particles on the

data of hygroscopic growth and CCN activation and the method to correct CCN efficiency spectra are described in Appendix A1. The CCN activation diameters d_{act} were calculated from CCNC data using the function proposed by *Rose et al*. [2008].

$$f_{nCCN,DMA2/nCN,DMA2} = \frac{F_{max}}{2}\left[1 + \mathrm{erf}\left(\frac{d_{p,dry} - d_{act}}{\sigma\sqrt{2}}\right)\right] \quad (1)$$

Here, F_{max} is the value that $f\, n_{CCN,DMA2}/n_{CN,DMA2}$ approaches as $d_{p,dry}$ increases and σ is the standard deviation. Hereafter, the CCNC-derived d_{act} and σ are expressed as $d_{act,CCN}$ and σ_{CCN}, respectively. The SS in the CCNC was calculated to be 0.18%, 0.49%, and 0.95% from $d_{act,CCN}$ of ammonium sulfate particles, using the Köhler equation and incorporating the Pitzer model as described by *Mochida et al*. [2010].

For the atmospheric data, the CCN efficiency spectra of singly charged particles were obtained for particles at four g_{set} values (1.0, 1.1, 1.25, and 1.4) under three SS conditions (0.18%, 0.49%, and 0.95%). The corrections were the same as those used for calibration with the ammonium sulfate particles. In the data analysis, $n_{CN,DMA2}$ that correspond to $<$50 counts in 210 s were not used because of large uncertainties.

Ammonium sulfate particles were introduced to the HTDMA before and after atmospheric observation, to examine the *g* distributions at 16 sizes, from 20.2 to 359 nm, under dry and humidified conditions. Inversion calculation [*Mochida et al*., 2010] and lognormal fittings were used to calculate the ratios of fitted mode diameters under humidified versus dry conditions (i.e., *g* at ~85% RH). In most cases, the obtained *g* agreed with the values from *Tang and Munkelwitz* [1994] within 5%. The setting diameters of DMA2 were corrected based on the differences of sizing between DMA1 and DMA2. This was determined by introducing ammonium sulfate particles to the HTDMA under the dry condition of DMA2 and calculating the size dependence using a third-degree polynomial before the observation. Ammonium sulfate particles were introduced again after the observation and *g* for 16 sizes were found to agree within 1.1% of those before the observation.

The actual *g* of the particles selected according to g_{set} had some variation because of the width of the DMA transfer function. This was accounted for as follows. First, the *g* distributions in 11 time periods (Figure S1 in the supporting information) for 16 sizes were retrieved using the Twomey algorithm, according to the work by *Mochida et al*. [2010]. Figures 2a–2d show the probability density functions of *g* (*gf*-PDF) for particles with $d_{p,dry}$ of 28.9, 49.6, 102, and 209 nm and the HTDMA kernel functions, which represent the transfer function of the HTDMA for singly charged particles, with g_{set} of 1.0, 1.1, 1.25, and 1.4. Different from the work by *Mochida et al*. [2010], the kernel functions and distributions of *g* in the bins of 1/1024 per decade were used without the conversion to coarse bins. Next, the *gf*-PDF for particles classified according to g_{set} (*gf*-PDF_{gset}) was obtained by multiplying *gf*-PDF by the kernel functions of g_{set} and by normalizing the resulting distributions, as shown in Figures 2e–2h. The mean of *g* of particles selected in DMA2 (g_m) varied with the time and dry particle diameter; the mean ± standard deviation (or ranges) of g_m at g_{set} of 1.0, 1.1, 1.25, and 1.4 for 16 sizes were calculated to be 1.023 ± 0.006 (1.011–1.034), 1.081 ± 0.009 (1.065–1.094), 1.265 ± 0.011 (1.250–1.291), and 1.393 ± 0.032 (1.330–1.449), respectively. The differences of g_m from g_{set} depended on the particle size (from 24.1 to 359 nm) and were up to 2%. The differences of g_m averaged for different sizes (from 24.1 to 359 nm) from g_{set} were up to 9%.

In this study, the CCN efficiency spectra for particles with g_{set} were predicted from the measured distributions of *g* to assess the prediction of CCN activation of aerosol particles from the hygroscopicity data. The values of the CCN efficiency spectra (i.e., $n_{CCN,DMA2}/n_{CN,DMA2}$ of particles at each dry diameter and at specific g_{set}) were calculated by integrating *gf*-PDF_{gset} over bins having S_{crit} smaller than the SS conditions in CCNC (0.18%, 0.49%, and 0.95%). Using the single hygroscopic parameter κ (proposed by *Petters and Kreidenweis* [2007]) as expressed below, κ-Köhler theory is used for the prediction.

$$S(d_{p,wet}) = \frac{d_{p,wet^3} - d_{p,dry^3}}{d_{p,wet^3} - d_{p,dry^3}(1-\kappa)} \exp\left(\frac{4\sigma_s M_w}{RT\rho_w d_{p,wet}}\right) \quad (2)$$

$$g = \frac{d_{p,wet}}{d_{p,dry}} \quad (3)$$

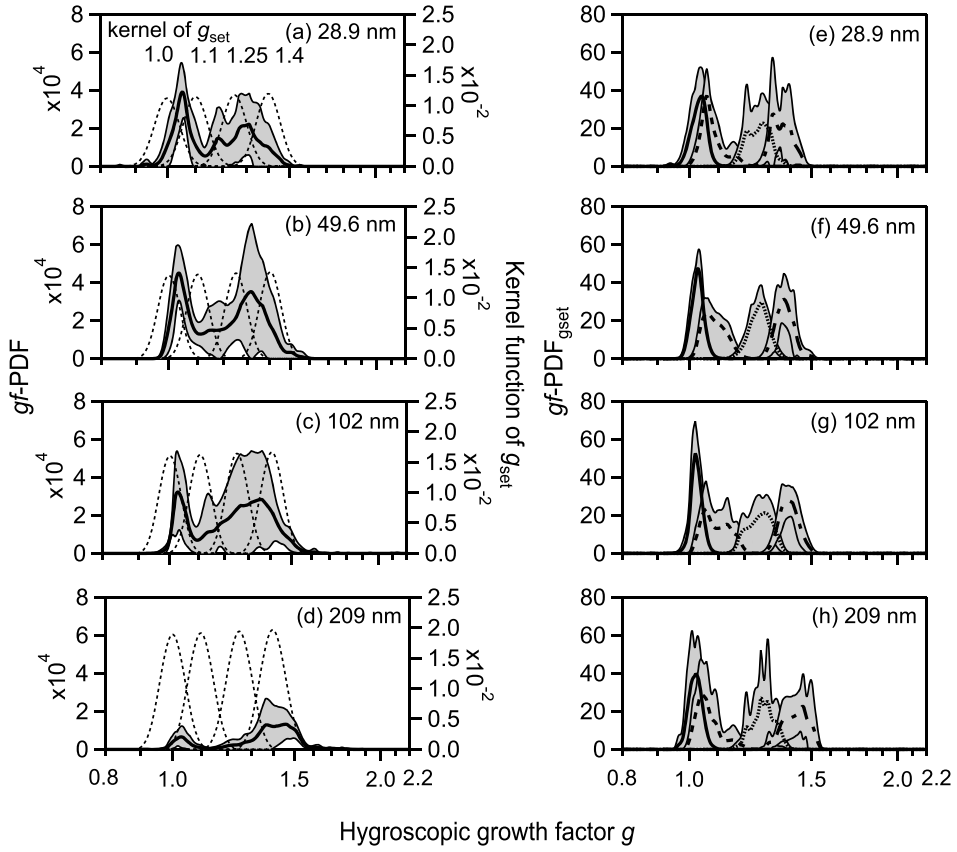

Figure 2. Log-spaced probability density functions of hygroscopic growth factors (*gf*-PDF) (mean: solid line, range of standard deviation: shaded area) and the HTDMA kernel functions for g_{set} of 1.0, 1.1, 1.25, and 1.4 and dry mobility diameter ($d_{p,dry}$) of (a) 28.9 nm, (b) 49.6 nm, (c) 102 nm, and (d) 209 nm. The estimated *gf*-PDF$_{gset}$ of particles downstream of the DMA2 with $d_{p,dry}$ of (e) 28.9 nm, (f) 49.6 nm, (g) 102 nm, and (h) 209 nm. The lines represent *gf*-PDF$_{gset}$ for particles with g_{set} of 1.0 (solid line), 1.1 (dotted line), 1.25 (dashed line), and 1.4 (dash-dotted line). The shaded areas represent the range of the standard deviation. The shaded areas with negative values of *gf*-PDF and *gf*-PDF$_{gset}$ are not shown.

Here, σ_s is the surface tension, M_w is the molecular weight of water, R is the universal gas constant, T is the absolute temperature, ρ_w is the density of water, and $d_{p,wet}$ is the diameter of particles after humidification. S_{crit} of CCN was calculated as follows. First, κ was calculated using equations (2) and (3) with S ($d_{p,wet}$) of 0.85 and $d_{p,dry}$ and $d_{p,wet}$, the mobility diameters of particles in DMA1 and DMA2 of HTDMA, respectively. Next, the maximum of S ($d_{p,wet}$) (i.e., S_{crit}) was computed iteratively using the calculated κ. For this calculation of κ from g at 85% RH, T was assumed to be 301 K, the mean temperature of the sheath flow exiting DMA2 during the observation. For the calculation of S_{crit}, T was assumed to be 302 K, the mean temperature of the top column of the CCNC during the observation. For both of the calculations, σ_s were assumed to be that of pure water. The CCN activation diameters ($d_{act,g85}$) were then predicted using equation (1). Strictly, the distributions of dry mobility diameters of particles selected in DMA2 could skew as compared with those selected in DMA1 depending on the g distributions of particles selected in DMA1 and g_{set}. This effect was not taken into account in the analysis. The relative standard deviation of Gaussian curves fitted to the transfer functions of DMA1 at 16 $d_{p,dry}$ settings, that is, the indicator of the size distributions of dry particles selected in DMA1, is small (3%) as compared with the variations of CCN activation diameters calculated by different methods (Figure 8). Therefore, the above effect was presumably not important for the main discussion.

2.3. Cloud Parcel Model

The cloud parcel model used in this study has been explained elsewhere [*Takeda and Kuba*, 1982; *Kuba and Takeda*, 1983; *Kuba et al*., 2003]. Here the calculation scheme has been modified from the previous versions by calculating the growth and activation of particles by κ-Köhler theory.

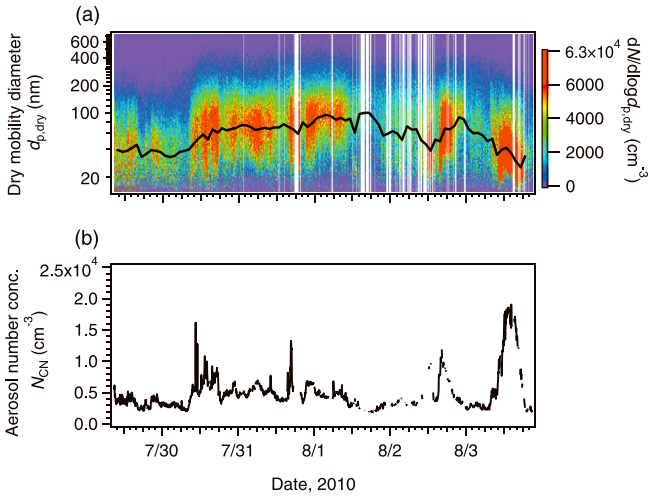

Figure 3. Time series of (a) the number-size distributions and (b) the total number concentrations (14.1–711 nm) of aerosol particles. The black line in Figure 3a is the mode diameters derived from single lognormal fittings.

In the cloud parcel model, N_{cd} and R_{eff} were calculated at updraft velocities (v) of 0.1, 0.5, 1.0, and 5.0 m s^{-1} as an air parcel rises 100 m adiabatically from the cloud base at 500 m AGL. The input data to the model were the cumulative number-size distributions of aerosol particles. The HTDMA and SMPS data were used for the preparation of the input data. In the base case of the model, all the aerosol particles in the range of $0.8 \le g \le 2.2$ were considered. In some other model cases, only a portion of particles in specific ranges of g were assumed to be present. The hygroscopic parameter κ of all particles with $d_{p,dry}$ from 20.2 to 359 nm was converted to that of pure ammonium sulfate (κ: 0.61) [*Petters and Kreidenweis*, 2007], with the conversion of the diameter so as to have the same S_{crit} based on the κ-Köhler theory. The conversion was performed for particles with g and $d_{p,dry}$ in the resolutions of 64 and 16 bins per decade, respectively. For each bin, the midpoint values of g and $d_{p,dry}$ on the log scale were used. The cumulative number-size distributions for these particles were then calculated based on the conversion. For particles larger than 359 nm (up to 18.8 μm), the cumulative number-size distributions were estimated by extrapolation using lognormal fittings to the number-size distributions measured using the SMPS (from 14.1 to 711 nm). All particles larger than 359 nm were treated as ammonium sulfate without the conversion of the diameters. Uncertainty associated with the extrapolation, with the assumption of κ, is presumably small, as explained in Appendix A2. Based on the above calculations, the contribution of particles with different hygroscopicity to the cloud droplet formation was evaluated. In the model calculations of the base case, corrections for the difference of the CCN activation diameters using the HTDMA and CCNC and the presence of CCN-inactive particles were made based on the results from the HTDMA and CCNC. In the case where the difference of the CCN activation diameters was considered in the model, κ at 85% RH (κ_{85}) and κ_{CCN} with different g were calculated from HTDMA-derived and CCNC-derived activation diameters using the following equations as well as equations (2) and (3).

$$K_e = \exp\left(\frac{4\sigma_s Mw}{RT\rho_w d_{p,wet}}\right) \tag{4}$$

$$\kappa_{85} = (g^3 - 1)\left(\frac{K_e}{0.85} - 1\right) \tag{5}$$

With the above corrections, the difference of the CCN activation diameters predicted from the HTDMA data and those measured using the CCNC was discussed.

3. Results and Discussion

3.1. Number-Size Distributions of Aerosol Particles

The time series of the number-size distributions and the total number concentrations of aerosol particles are presented in Figures 3a and 3b. As seen in Figure 3a, a large portion of particles were present in the Aitken mode range ($d_{p,dry} < 100$ nm). The mode diameters derived from fittings with a single lognormal curve was 60 ± 19 nm (mean ± SD). Fittings with two lognormal curves gave mean mode diameters of 34 ± 10 nm and 83 ± 18 nm (mean ± SD). The total number concentration of aerosols (N_{CN}) from 14.1 to 711 nm was 6932 ± 8379 cm^{-3} (mean ± SD). A plausible reason for the dominance of Aitken mode particles could be a large emission of POA in the studied urban area. According to other studies that characterized urban

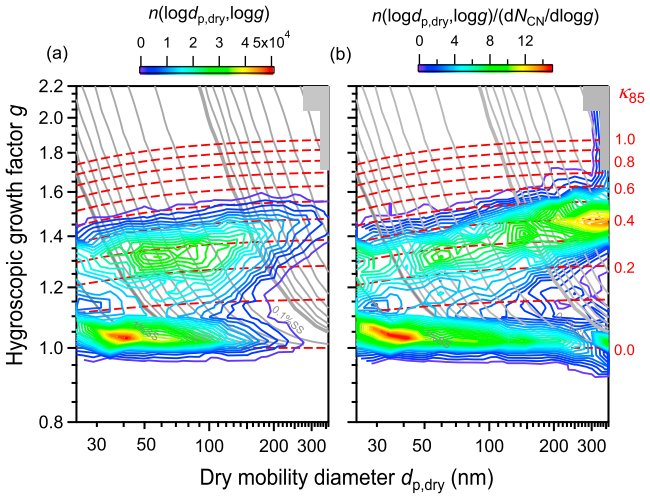

Figure 4. (a) Average two-dimensional distribution of the number concentrations of aerosol particles as a function of g and $d_{p,dry}$ at 85% RH and (b) the average of 11 normalized distributions. The dashed red lines represent contours of κ at 85% RH (κ_{85}). The gray contours show critical SS estimated from the κ-Köhler theory [*Mochida et al.*, 2011].

aerosols, hydrocarbon-like organic aerosol (HOA) is likely POA emitted by local combustion and these mainly exist in the Aitken mode. By contrast, oxygenated organic aerosol (OOA) is likely SOA and they mainly exist in the accumulation mode [*Zhang et al.*, 2005a, 2005b]. Another possible reason for the dominance of Aitken mode particles could be the occurrence of new particle formation. The increase of the number concentrations of small particles ($d_{p,dry} < 40$ nm) and the total number concentrations to $>10{,}000\ cm^{-3}$ during the observation implied an influence from new particle formation.

3.2. Distributions of Hygroscopic Growth Factors

The average distributions of g as a function of the particle diameter and the average of the normalized distributions are presented in Figures 4a and 4b, respectively. As seen in the figures, the average g distribution is characterized by the presence of less and more hygroscopic modes. Most of the individual distributions of g over the 11 time periods were bimodal as well, as shown in Figure S1.

The average of the number-size distributions and the average of the number fractions of aerosol particles in four different ranges of g are shown in Figures 5a and 5b. In this study, particles with ranges of $0.8 \le g < 1.1$ and $1.1 \le g < 1.25$ (i.e., $0.8 \le g < 1.25$) were defined as less hygroscopic particles and those with ranges of $1.25 \le g < 1.4$ and $1.4 \le g \le 2.2$ (i.e., $1.25 \le g \le 2.2$) were defined as more hygroscopic particles. As seen in Figure 5a, the concentrations of particles in the lowest hygroscopicity range ($0.8 \le g < 1.1$) had a maximum in the Aitken mode range ($d_{p,dry} < 100$ nm) and it decreased toward the accumulation mode range ($d_{p,dry} > 100$ nm). The number fractions of particles in this hygroscopicity range also had a maximum in the Aitken mode range (Figure 5b). By contrast, the concentrations and the number fraction of particles in the highest hygroscopicity range ($1.4 \le g \le 2.2$) in the accumulation mode range were substantially higher compared to those in the Aitken mode range. In the case of the particles in the range of $1.1 \le g < 1.25$, while the shape of the number-size distributions was similar to that of the particles in the lowest hygroscopic range, the size dependence of the number fraction was small.

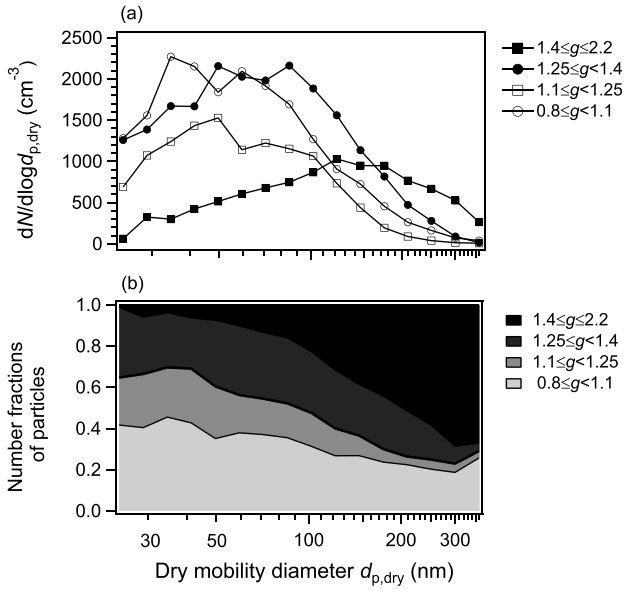

Figure 5. (a) Average of the number-size distributions and (b) the average of the number fractions of aerosol particles in the ranges of $0.8 \le g < 1.1$, $1.1 \le g < 1.25$, $1.25 \le g < 1.4$, and $1.4 \le g \le 2.2$.

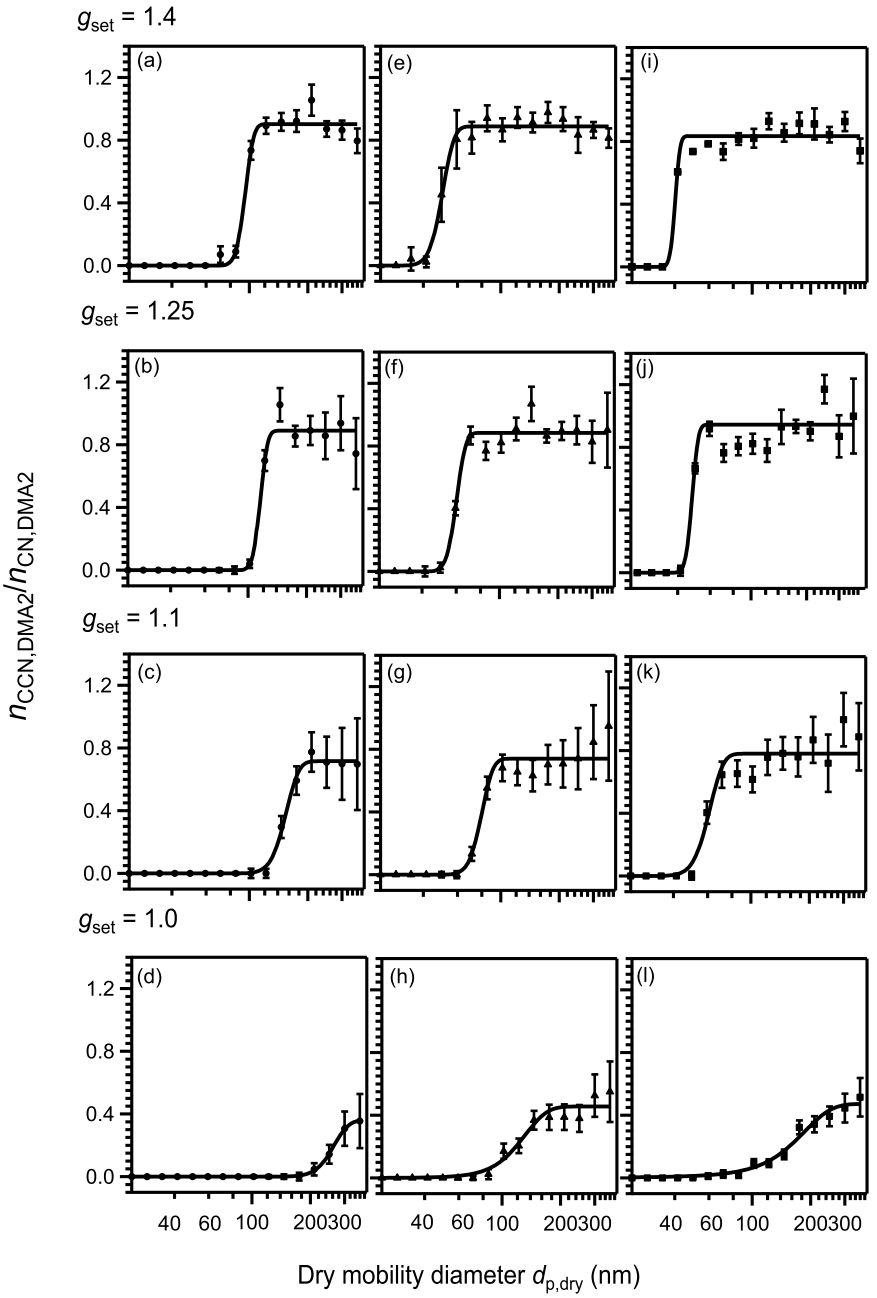

Figure 6. The averages of the measured CCN efficiency spectra (symbols) and the curves fitted to the averages (solid lines) for aerosol particles with g_{set} of (a, e, and i) 1.4, (b, f, and j) 1.25, (c, g, and k) 1.1, and (d, h, and l) 1.0 at 0.18% (Figures 6a–6d), 0.49% (Figures 6e–6h), and 0.95% (Figures 6i–6l) SS. The bars represent the standard deviation.

The less hygroscopic particles may have consisted of black carbon (BC) or primary-emitted HOA, as can be inferred from their compositional characteristics. Furthermore, the high abundance of less hygroscopic particles in the Aitken mode range also supported the contribution of BC and HOA, as discussed in section 3.1. More hygroscopic particles may have consisted of secondary-generated OOA and inorganics as has been suggested for urban aerosols (Tokyo) by *Mochida et al.* [2008]. Aerosols from the East Asian continent [*Aikawa et al.*, 2010; *Yoshitomi et al.*, 2011] as well as those from other parts of Japan might have contributed to the observed more hygroscopic particles, as suggested from the 5 day backward air mass trajectories (Figure S2) passing near the coast of China. This interpretation is also supported by observation that aerosols from China by the long-range

Table 1. Parameters of the Function (Equation (1)) Fitted to the Averages of the Measured CCN Efficiency Spectra for Atmospheric Particles Selected With Specific g_{set} Values and Ammonium Sulfate Particles

Particle Type	g_{set}[a]	SS[b] (%)	F_{max}[c]	$d_{act,CCN}$[d] (nm)	σ_{CCN}[e]	$\sigma_{CCN}/d_{act,CCN}$
Atmospheric aerosols	1.0	0.18	0.36	239.0	40	0.16
		0.49	0.46	123.1	33	0.27
		0.95	0.47	139.4	51	0.36
	(mean)		0.43		42	0.26
	1.1	0.18	0.72	152.7	20	0.13
		0.49	0.74	79.3	9.1	0.11
		0.95	0.78	50.7	7.2	0.14
	(mean)		0.75		12	0.13
	1.25	0.18	0.89	115.6	8.0	0.07
		0.49	0.88	60.0	5.4	0.09
		0.95	0.95	40.1	2.5	0.06
	(mean)		0.91		5.3	0.07
	1.4	0.18	0.90	95.0	7.8	0.08
		0.49	0.89	49.9	5.8	0.11
		0.95	0.83	33.7	1.6	0.01
	(mean)		0.88		5.1	0.08
Ammonium sulfate		0.18	0.99	86.3	3.9	0.05
		0.49	0.98	45.3	1.3	0.03
		0.95	0.98	29.7	0.7	0.02
	(mean)		0.98		2.0	0.03

[a] Setting hygroscopic growth factors.
[b] Supersaturations in the CCNC.
[c] The value that $fn_{CCN,DMA2}/n_{CN,DMA2}$ approaches as $d_{p,dry}$ increases.
[d] CCN activation diameters.
[e] The standard deviation of the fitting function.

transport had high hygroscopic growth factors in Okinawa, Japan [*Mochida et al.*, 2010]. The finding in this study that the size distribution of more hygroscopic particles is characterized by the larger size than that of less hygroscopic particles was reasonable because more hygroscopic particles may have grown by condensation, coagulation, and in-cloud processes during the long-range transport. Further, the growth from less hygroscopic to more hygroscopic particles in the local urban air is also possible. *Wang et al.* [2010] reported that the hygroscopicity of nonhygroscopic particles (fresh POA or BC) increased within a few hours during the daytime by the condensation of photochemically formed SOA in Mexico. This process could also explain the size dependence of the number fractions of particles with different g (Figure 5b).

The individual distributions of g over the 11 time periods (Figure S1) were mainly bimodal as was also the case of the average distribution. However, in some cases the separation in the mode was not clear, while in others, only the less hygroscopic mode was clearly observed. The substantial variation in the distributions of g in Nagoya was in contrast to the unimodal distributions observed at remote locations to the east (the western North Pacific) and to the west (Okinawa) of Nagoya [*Mochida et al.*, 2010, 2011]. The variation may have been influenced by different degrees of mixing of air masses with different origins or local formation of SOA and subsequent aging.

3.3. CCN Efficiency Spectra of Aerosol Particles With Different Hygroscopic Growth Factors

Figures 6a–6l show the averages of the measured CCN efficiency spectra and the curves fitted to the averages for aerosol particles with four different g_{set} (1.0, 1.1, 1.25, and 1.4). The parameters obtained by the fitting using equation (1) (i.e., F_{max}, $d_{act,CCN}$, σ_{CCN}, and $\sigma_{CCN}/d_{act,CCN}$) are summarized in Table 1. The $\sigma_{CCN}/d_{act,CCN}$ values are the measures of the heterogeneity of aerosol particles; the higher the value, the less uniform are the particles [*Rose et al.*, 2008, 2010]. Although the σ values are broadened by the widths of the transfer functions of two DMAs in HTDMA, this effect is not considered in this study.

In the case of more hygroscopic particles with g_{set} of 1.25 and 1.4, $n_{CCN,DMA2}/n_{CN,DMA2}$ increased sharply with increasing dry diameter (Figures 6a, 6b, 6e, 6f, 6i, and 6j) as represented by small $\sigma_{CCN}/d_{act,CCN}$ values (Table 1). The mean values of $\sigma_{CCN}/d_{act,CCN}$ for particles with g_{set} of 1.25 and 1.4 were 0.07 and 0.08, respectively, which were similar to the values of ammonium sulfate particles. The $d_{act,CCN}$ of more

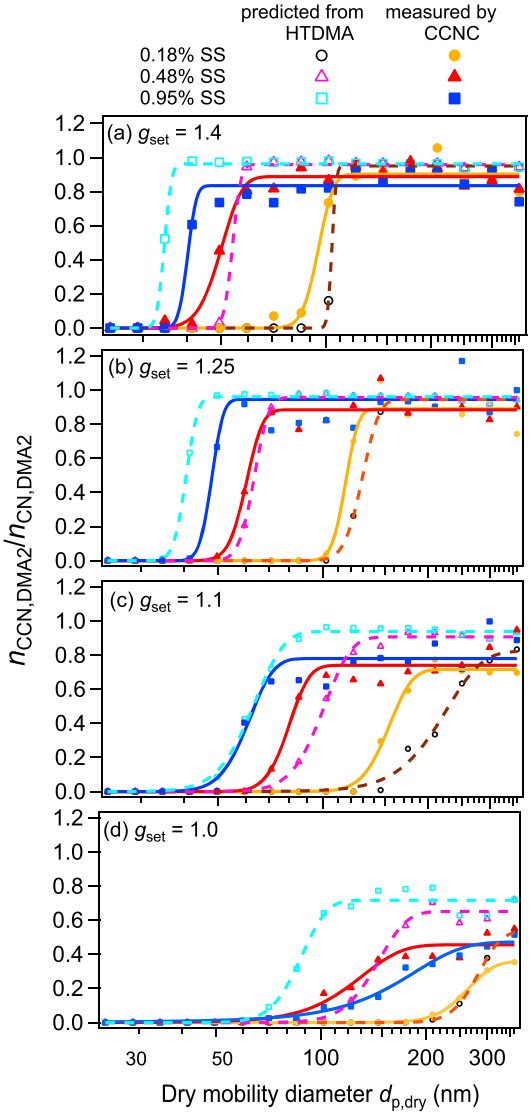

Figure 7. The averages of the CCN efficiency spectra predicted from the distribution of g at 85% RH (open symbols) and those measured using the CCNC (solid symbols) for aerosol particles with g_{set} of (a) 1.4, (b) 1.25, (c) 1.1, and (d) 1.0. The dashed and solid lines represent the curves fitted to the averages of the predicted and measured spectra, respectively.

hygroscopic particles were smaller than those of less hygroscopic particles with g_{set} of 1.0 and 1.1 at respective SS conditions (Figures 6c, 6d, 6g, 6h, 6k, and 6l), indicating high CCN activity as expected from higher g_{set}. F_{max} values were close to 1.0, indicating that particles well above $d_{act,CCN}$ were mostly activated. Both $\sigma_{CCN}/d_{act,CCN}$ values similar to that of ammonium sulfate and high F_{max} values suggested that the hygroscopicity at 85% RH was tightly linked to the CCN activity of particles under supersaturated conditions.

In the case of particles with g_{set} of 1.0, the increase of $n_{DMA2,CCN}/n_{DMA2,CN}$ with increasing dry diameter was not as sharp (Figures 6d, 6h, and 6l). The mean $\sigma_{CCN}/d_{act,CCN}$ was 0.26, which was substantially larger than that for more hygroscopic particles. This large $\sigma_{CCN}/d_{act,CCN}$ is hypothesized to be caused in part by the fact that the hygroscopicity κ of particles with g_{set} of 1.0 can vary by many orders of magnitude (the order of κ can be infinitely low). It is consistent with the result that the CCN-effective spectrum predicted by HTDMA data also has the same tendency (large $\sigma_{CCN}/d_{act,CCN}$ of less hygroscopic particles) as shown in Figure 7 (see the next section). The $d_{act,CCN}$ were also larger than those for more hygroscopic particles, indicating low CCN activity as expected from low g_{set}. F_{max} values were much less than 1.0: 0.36, 0.46, and 0.47 at 0.18%, 0.49%, and 0.95% SS, respectively. This finding showed that the fractions of inactive particles were high even in the case of high SS and large particles within the measured size range. The low F_{max} values indicated either that the hygroscopicity of less hygroscopic particles was not uniform (in time as well as size, because the result was from the averages of multiple measurements) or that the asphericity of particles showed large variation. The nonuniformity or asphericity of particles may also affect the large $\sigma_{CCN}/d_{act,CCN}$ values in part. However, we did not obtain the contribution quantitatively.

In the case of particles with g_{set} of 1.1 (Figures 6c, 6g, and 6k), the above mentioned characteristics of particles with g_{set} of 1.0 (i.e., moderate increase of $n_{DMA2,CCN}/n_{DMA2,CN}$ versus $d_{p,dry}$ and F_{max} values substantially less than unity) were observed, although their patterns were not as clear as particles with g_{set} of 1.0. The CCN-inactive particles with g_{set} of 1.0 and 1.1, as evidenced by F_{max} values less than unity, may have been fresh and uncoated BC. Previous studies in urban sites had suggested that these particles have the lowest CCN activity among particles with the same mobility diameters [*Kuwata and Kondo*, 2008; *Rose et al.*, 2010].

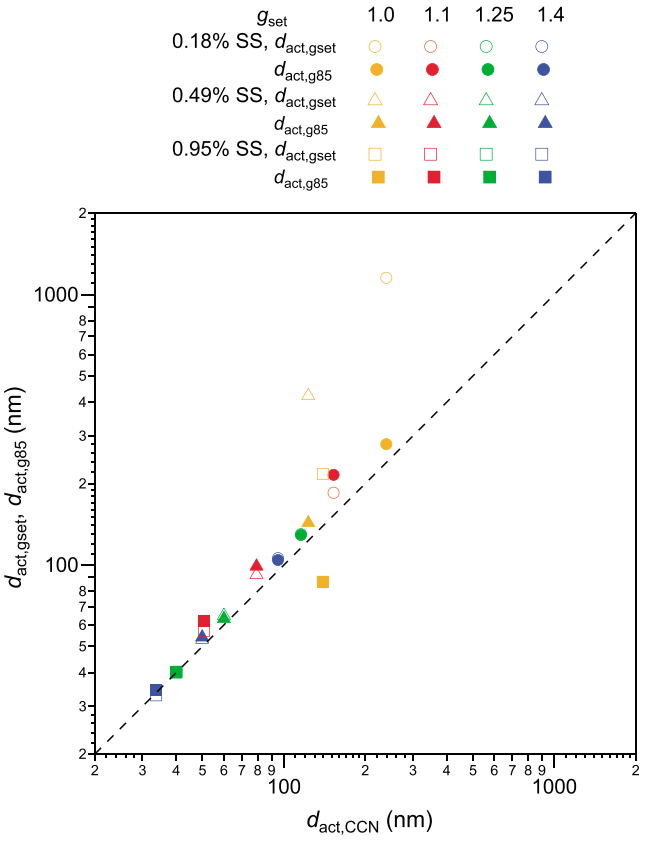

Figure 8. The CCN activation diameters predicted from g_{set} with and without consideration of the width of the transfer function of DMA1 (i.e., $d_{act,g85}$ and $d_{act,gset}$, respectively) plotted against the measured CCN activation diameters ($d_{act,CCN}$). These values were obtained from the fittings to the averages of the predicted and measured CCN efficiency spectra.

3.4. Prediction of CCN Activation Diameters From Hygroscopic Growth Factor Distributions and Comparison to Measured Activation Diameters

To examine the prediction of the CCN activation of aerosol particles from measured hygroscopicity, the CCN efficiency spectra were estimated from the measured distributions of g. The averages of the predicted CCN efficiency spectra at each SS condition and the curves fitted to the averages using equation (1), for aerosol particles with four different g_{set} (1.0, 1.1, 1.25, and 1.4) are present in Figure 7, together with the averages of measured CCN efficiency spectra and the curves fitted to them (see Figure S3 for the standard deviation). Here, particles in the range of $0.8 \le g < 1.0$ were assumed to be CCN-inactive. The figure shows that the differences of the shapes of CCN efficiency spectra caused by the difference of g_{set} were predicted to some extent. The $\sigma_{g85}/d_{act,g85}$, where σ_{g85} and $d_{act,g85}$ are, respectively, σ and d_{act} obtained by the fitting of the predicted CCN efficiency spectra presented in Figure S3, for more hygroscopic particles with g_{set} of 1.25 and 1.4 were on average very small (0.08 and 0.04, respectively) as in the case of $\sigma_{CCN}/d_{act,CCN}$ (0.07 and 0.08, respectively). In contrast, less hygroscopic particles with g_{set} of 1.0 and 1.1 had on average a large $\sigma_{g85}/d_{act,g85}$ (0.16 and 0.19, respectively) as in the case of $\sigma_{CCN}/d_{act,CCN}$ (0.26 and 0.13, respectively). The prediction of the CCN efficiency spectra was, however, rather poor for particles with g_{set} of 1.0 (Figure 7d), which was possibly caused by the asphericity of the particles (aggregate or fractal structures). Quantitative evaluation of the F_{max} values prediction was not performed because the validity of the estimation of CCN-inactive particles from $g < 1.0$ was not clear.

The relation between $d_{act,CCN}$ derived from the averages of measured CCN efficiency spectra and the activation diameters predicted from the distributions of g ($d_{act,g85}$) is presented in Figure 8. The $d_{act,CCN}$ were smaller than $d_{act,g85}$ with one exception, indicating that the measured CCN activity was higher than that predicted from the hygroscopicity data. In particular, plots for less hygroscopic particles showed large deviations from the 1:1 line. The mean values of $d_{act,g85}$, $d_{act,CCN}$, and the activation diameters predicted from g_{set} of 1.0, 1.1, 1.25, and 1.4 ($d_{act,gset}$) are summarized in Table 2. Whereas $d_{act,g85}$ from $d_{act,CCN}$ agreed within 12% for more hygroscopic particles, the disagreement was larger (16%–41%) for less hygroscopic particles. Figure 8 and Table 2 also show the relationship between $d_{act,CCN}$ and $d_{act,gset}$, the value without the correction for the width of g. While $d_{act,gset}$ and $d_{act,g85}$ agreed within 4% for more hygroscopic particles, the disagreement was very large (7%–412%) for less hygroscopic particles. The results in Figure 8 show that taking the width of g into consideration shifts the plots toward the 1:1 line. Hence, this consideration is probably important for the precise prediction of CCN activation diameters, although the effect of the skews of dry diameter distributions of particles in DMA2 (section 2.2) are not evaluated in a fully quantitative

Table 2. Summary of Predicted and Measured CCN Activation Diameters and Other Values Derived From the Activation Diameters

g_{set}[a]	SS[b] (%)	$d_{act,gset}$[c] (nm)	$d_{act,g85}$[d] (nm)	$d_{act,CCN}$[e] (nm)	κ_{gset}[f]	κ_{85}[g]	κ_{CCN}[h]	$d_{act,g85}/d_{act,CCN}$	$d_{act,gset}/d_{act,g85}$	$d_{act,gset}/d_{act,CCN}$
1.0	0.18	1153	279.9	239.0	0	0.018	0.029	1.17	4.12	4.82
	0.49	422	143.1	123.1	0	0.016	0.026	1.16	2.95	3.43
	0.95	217	86.7	139.4	0	0.018	0.002	0.62	2.50	1.56
(Mean)					0	0.017	0.019	0.99	3.19	3.27
1.1	0.18	185	215.4	152.7	0.062	0.040	0.112	1.41	0.86	1.21
	0.49	92	98.8	79.3	0.066	0.054	0.105	1.25	0.93	1.16
	0.95	57	62.1	50.7	0.071	0.055	0.106	1.22	0.92	1.12
(Mean)					0.066	0.050	0.108	1.29	0.90	1.17
1.25	0.18	130	129.1	115.6	0.183	0.187	0.260	1.12	1.01	1.12
	0.49	65	63.3	60.0	0.197	0.210	0.246	1.06	1.03	1.08
	0.95	40	40.3	40.1	0.215	0.214	0.218	1.00	0.99	1.00
(Mean)					0.198	0.204	0.241	1.06	1.01	1.07
1.4	0.18	106	104.3	95.0	0.336	0.355	0.468	1.10	1.02	1.12
	0.49	53	54.1	49.9	0.366	0.340	0.430	1.08	0.98	1.06
	0.95	33	34.5	33.7	0.401	0.346	0.370	1.02	0.96	0.98
(Mean)					0.368	0.347	0.423	1.07	0.98	1.05

[a] Setting hygroscopic growth factors.
[b] Supersaturations in the CCNC.
[c] CCN activation diameters predicted from g_{set} without consideration of the width of the transfer function of DMA1.
[d] Same as c but with consideration of the width of the transfer function of DMA1.
[e] CCN activation diameters measured using the CCNC.
[f] Values of κ calculated from $d_{act,gset}$.
[g] Same as f but calculated from $d_{act,g85}$.
[h] Same as f but calculated from $d_{act,CCN}$.

manner. CCN activation diameters calculated from independent measured and predicted CCN efficiency spectra (not from the averages) i.e., $d'_{act,CCN}$ and $d'_{act,g85}$, respectively, were also obtained (Figure S4). The mean values are similar to the result obtained by use of average CCN efficiency spectra in Figure 8 (within 15% except for one point for particles with g_{set} of 1.0 at 0.49% SS). These data were not used for the analysis in this section because some of the fittings to the predicted CCN efficiency spectra failed or resulted in exceptional curves.

However, the width of g does not fully explain the discrepancy from the 1:1 line. A possible cause of the differences between $d_{act,g85}$ and $d_{act,CCN}$ was the surface tension reduction caused by organics. Based on analysis of filter extracts, the surface tension reduction was reported to be approximately 25% in the Po Valley [*Facchini et al.*, 2000] and 5%–22% in Mexico [*Padró et al.*, 2010]. Given that the percentage decrease of CCN activation diameters by the surface tension with respect to that of water was comparable to the percentage decrease of the surface tension itself [*Wex et al.*, 2008], the expected range of the decrease of CCN activation diameters by surface tension was estimated to be approximately 5%–25% in the atmosphere.

Other possible causes of the differences between $d_{act,g85}$ and $d_{act,CCN}$ originate from the effects of solutes. The κ values vary up to ~20%, depending on the concentrations of aqueous solutions (corresponding to ~7% in CCN activation diameters). For example, in ammonium sulfate particles, κ calculated from g at ~90% RH (0.53) was 13% smaller than that calculated from CCN measurements (0.61) [*Petters and Kreidenweis*, 2007]. *Kreidenweis et al.* [2008] reported that the water contents computed from κ parameterization $(V_w/V_s)_\kappa$ and those from the Aerosol Inorganic Model [*Clegg et al.*, 1998] $(V_w/V_s)_{AIM}$ for some inorganics and organics agreed within ~20% at RH > 85% (based on an assessment of up to 99% RH). Hence, the deviation of κ was estimated to be within ~20% at RH > 85%. The influence of sparingly soluble components with degree of dissolution that depends on the water content in particles is potentially great. *Wex et al.* [2009] reported a large increase in g of laboratory-generated pure SOA particles at RH > 98%, suggesting possible overestimation of CCN activation diameters based on the measured g at 85% RH. Moreover, the sensitivity of mobility diameter to water uptake depends on the particle shape. *Tritscher et al.* [2011] reported that the measurement based on the mobility diameter using the DMA led to underestimation of the hygroscopicity for soot particles because of morphology changes.

While small differences of $d_{act,g85}$ from $d_{act,CCN}$ for more hygroscopic particles can be explained by either or both the surface tension reduction and the underestimation of the amount of solutes, it is difficult to explain

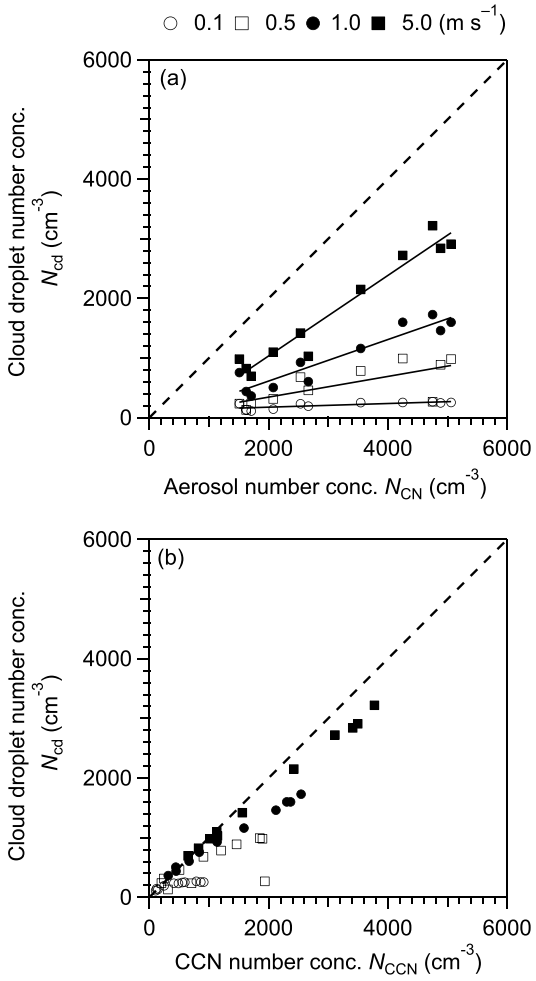

Figure 9. The plots of (a) N_{CN} and (b) N_{CCN} against the cloud droplet number concentrations N_{cd}. The results are from the base case of the cloud parcel model with v of 0.1 (open circles), 0.5 (open squares), 1.0 (solid circles), and 5.0 m s^{-1} (solid squares).

the differences for less hygroscopic particles by surface tension reduction alone. Although it was not clear which mechanism was the main contribution to the differences, the results indicated that the amounts of soluble materials in less hygroscopic particles were larger than those estimated from the measured hygroscopic growth at 85% RH.

Assuming the surface tension of pure water and a spherical particle shape, the mean values of κ_{CCN} calculated from $d_{act,CCN}$ on particles with g_{set} of 1.0, 1.1, 1.25, and 1.4 were 0.02, 0.11, 0.24, and 0.42, respectively (Table 2). In contrast, the mean values of κ_{85} calculated from $d_{act,g85}$ for particles with g_{set} of 1.0, 1.1, 1.25, and 1.4 were 0.02, 0.05, 0.20, and 0.35, respectively. While the mean values of κ_{CCN} were 1.0–1.4 times κ_{85} for more hygroscopic particles with g_{set} of 1.25 and 1.4, the mean values of κ_{CCN} were 0.1–2.8 times κ_{85} for less hygroscopic particles with g_{set} of 1.0 and 1.1. The differences of κ_{CCN} from κ_{85} for less hygroscopic particles were in general larger than those of more hygroscopic particles as was expected from the comparison in Figure 8.

The finding that κ_{CCN} of less hygroscopic particles were larger than κ_{85} strongly suggested the presence of a hydrophilic component that could not be detected accurately using the HTDMA. If particles are assumed to be ammonium sulfate with κ of 0.58 (derived from the calibration of the CCNC) with an insoluble component with κ of 0, the mean values and ranges of the soluble component volume fractions (ε_{sol}) in particles with g_{set} of 1.0 and 1.1 are calculated to be 3.0% (2.8%–3.3%) and 8.6% (6.3%–10%), respectively. If the soluble component in the particles are OOA or SOA ($\kappa \sim 0.1$), the mean values and ranges of ε_{sol} are calculated to be 17% (16%–18%) and 50% (40%–55%) for particles with g_{set} of 1.0 and 1.1, respectively. This suggests that the fraction of soluble components in less hygroscopic particles could be substantial, depending on the hygroscopicity of the chemical components.

3.5. Prediction of Cloud Droplet Formation and Growth From Hygroscopic Growth Factor Distributions

In the base case of the cloud parcel model, the cloud droplet number concentrations (N_{cd}) and the effective radius (R_{eff}) were estimated from the distributions of g, which were measured using the HTDMA. Further, the number concentrations of CCN (N_{CCN}) at the maximum SS in the model (S_{max}) were estimated. The average SS profiles for four updraft velocities (v) had a maximum at ~530 m AGL and showed rapid decreases above that height. S_{max} depended on the updraft velocity and the total number concentrations of aerosol particles (N_{CN}); the mean values of S_{max} at v of 0.1, 0.5, 1.0, and 5.0 m s^{-1} were 0.15%, 0.34%, 0.48%, and 1.1%, respectively. Figure 9a shows N_{CN} versus N_{cd} in the base case for 11 time periods (Figure S1) under different conditions of v. Whereas N_{cd} depended on v and N_a if v was high, N_{cd} remained small if v was low. This

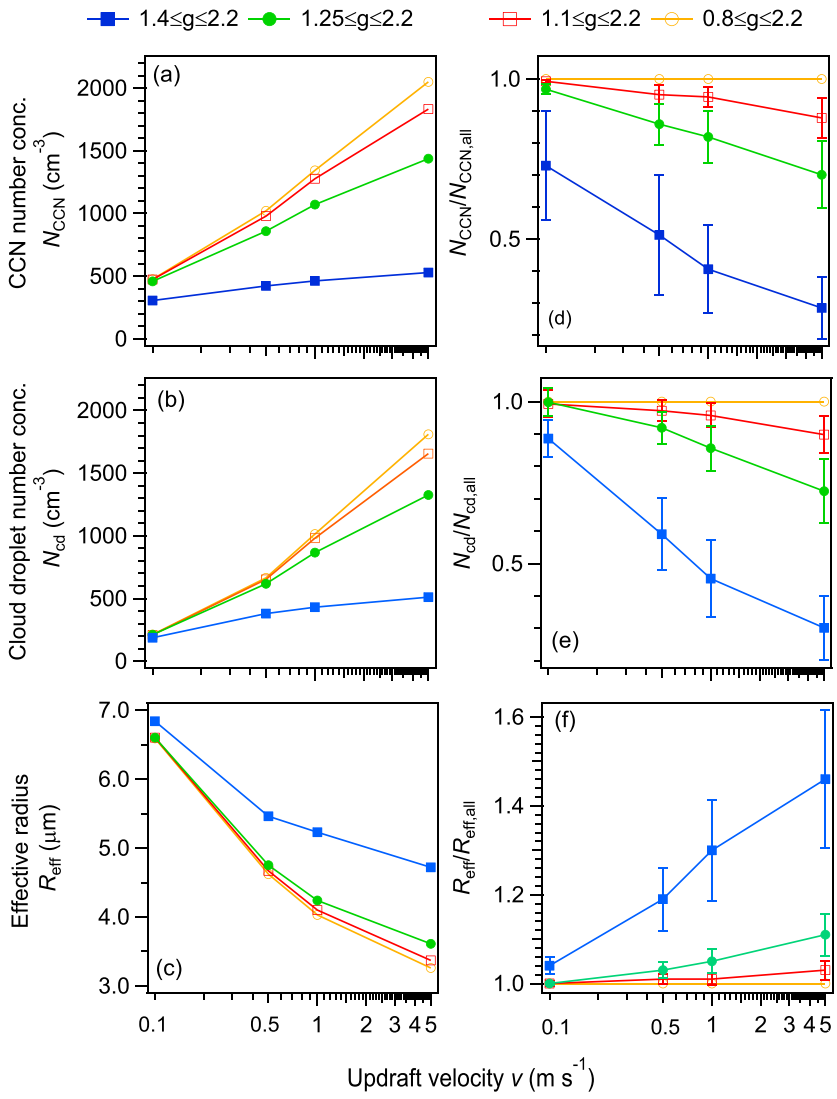

Figure 10. Mean values of (a) N_{CCN}, (b) N_{cd}, and (c) R_{eff} with consideration of particles in different ranges of g (blue: $1.4 \le g \le 2.2$, green: $1.25 \le g \le 2.2$, red: $1.1 \le g \le 2.2$, and yellow: $0.8 \le g \le 2.2$) and the means and standard deviations of (d) $N_{CCN}/N_{CCN,all}$, (e) $N_{cd}/N_{cd,all}$, and (f) $R_{eff}/R_{eff,all}$. $N_{CCN,all}$, $N_{cd,all}$, and $R_{eff,all}$ denote N_{CCN}, N_{cd}, and R_{eff} in the case of $0.8 \le g \le 2.2$.

indicated that the former was in aerosol- and updraft-sensitive regimes and that the latter was in an updraft-limited regime [*Reutter et al.*, 2009]. Figure 9b shows N_{CCN} (in hypothetical equilibrium conditions at S_{max}) versus N_{cd}. The hypothetical CCN at S_{max} were not all activated as cloud droplets, particularly in the cases of low v and large N_{CCN}. This result may be associated with the kinetic mechanism not all particles grow to become cloud droplets even if S_{crit} of particles is smaller than S_{max}, because of the insufficient time to activate [*Nenes et al.*, 2001].

Model calculations in the base case showed that corrections for the difference of $d_{act,g85}$ from $d_{act,CCN}$ (section 3.4) and the presence of CCN-inactive particles (section 3.3) based on the results from the HTDMA and the CCNC, had a small influence on the cloud droplet formation. The difference of $d_{act,g85}$ from $d_{act,CCN}$ was considered so that particles in the ranges of $0.8 \le g < 1.1$, $1.1 \le g < 1.25$, $1.25 \le g < 1.4$, and $1.4 \le g \le 2.2$ had κ_{CCN} (Table 2) if their original κ_{85} were lower than κ_{CCN}. Further, the presence of CCN-inactive particles (F_{max} values less than unity) with g_{set} of 1.0 and 1.1 (Table 1) was also considered by multiplying the number concentrations of particles in the ranges of $0.8 \le g < 1.05$ and $1.05 \le g \le 1.15$ by 0.43 and 0.75, respectively. If model calculations were performed without the corrections for the difference of $d_{act,g85}$ from $d_{act,CCN}$ and the presence of CCN-inactive particles, N_{CCN}, N_{cd}, and R_{eff} at v of 1.0 m s^{-1} (or 5.0 m s^{-1}) changed within 2% (5%), 2% (5%), and 1% (2%), respectively. The very

Table 3. Mean and Standard Deviation of N_{CCN}, N_{cd}, and R_{eff}, and the Ratios of N_{CCN}, N_{cd}, and R_{eff} to Those in the Case of $0.8 \le g \le 2.2$ ($N_{CCN,all}$, $N_{cd,all}$, and $R_{eff,all}$)

v[a]	0.1 m s^{-1}	0.5 m s^{-1}	1.0 m s^{-1}	5.0 m s^{-1}
N_{CCN}[b] base case ($0.8 \le g \le 2.2$)	476 ± 298 (+4%)	1024 ± 684 (+19%)	1358 ± 867 (+27%)	2061 ± 1211 (+43%)
$1.1 \le g \le 2.2$	473 ± 296 (+3%)	979 ± 666 (+14%)	1277 ±836 (+19%)	1832 ±1139 (+27%)
$1.25 \le g \le 2.2$	458 ± 283	859 ± 567	1071 ± 677	1437 ± 897
$1.4 \le g \le 2.2$	306 ± 151 (−33%)	423 ± 202 (−51%)	462 ± 228 (−57%)	529 ± 279 (−63%)
N_{cd}[c] base case ($0.8 \le g \le 2.2$)	212 ± 57 (+1%)	665 ± 302 (+8%)	1014 ± 516 (+18%)	1809 ± 969 (+36%)
$1.1 \le g \le 2.2$	211 ± 56 (+0%)	652 ± 307 (+6%)	981 ± 517 (+13%)	1655 ± 945 (+25%)
$1.25 \le g \le 2.2$	211 ± 56	617 ± 292	866 ± 447	1326 ± 772
$1.4 \le g \le 2.2$	187 ± 49 (−11%)	379 ± 157 (−38%)	431 ± 187 (−50%)	511 ± 258 (−62%)
R_{eff}[d] base case ($0.8 \le g \le 2.2$)	6.59 ± 0.6 (−0%)	4.62 ± 0.8 (−3%)	4.03 ± 0.7 (−5%)	3.26 ± 0.6 (−10%)
$1.1 \le g \le 2.2$	6.60 ± 0.6 (−0%)	4.67 ± 0.8 (−2%)	4.10 ± 0.8 (−3%)	3.37 ± 0.6 (−7%)
$1.25 \le g \le 2.2$	6.60 ± 0.6	4.75 ± 0.9	4.24 ± 0.8	3.61 ± 0.7
$1.4 \le g \le 2.2$	6.84 ± 0.7 (+4%)	5.46 ± 0.9 (+15%)	5.23 ± 0.9 (+23%)	4.72 ± 0.8 (+31%)
$N_{CCN}/N_{CCN,all}$ base case ($0.8 \le g \le 2.2$)	1.00	1.00	1.00	1.00
$1.1 \le g \le 2.2$	0.99 ± 0.01 (−1%)	0.95 ± 0.03 (−5%)	0.93 ± 0.04 (−7%)	0.87 ± 0.07 (−13%)
$1.25 \le g \le 2.2$	0.97 ± 0.01 (−3%)	0.86 ± 0.06 (−14%)	0.81 ± 0.08 (−19%)	0.70 ± 0.11 (−30%)
$1.4 \le g \le 2.2$	0.73 ± 0.17 (−27%)	0.51 ± 0.19 (−49%)	0.40 ± 0.13 (−60%)	0.28 ± 0.10 (−72%)
$N_{Cd}/N_{Cd,all}$ base case ($0.8 \le g \le 2.2$)	1.00	1.00	1.00	1.00
$1.1 \le g \le 2.2$	0.99 ± 0.04 (−1%)	0.97 ± 0.03 (−3%)	0.96 ± 0.04 (−4%)	0.90 ± 0.06 (−10%)
$1.25 \le g \le 2.2$	0.99 ± 0.04 (−1%)	0.92 ± 0.05 (−8%)	0.86 ± 0.07 (−14%)	0.72 ± 0.10 (−28%)
$1.4 \le g \le 2.2$	0.89 ± 0.06 (−11%)	0.59 ± 0.11 (−41%)	0.45 ± 0.12 (−55%)	0.30 ± 0.10 (−70%)
$R_{eff}/R_{eff,all}$ base case ($0.8 \le g \le 2.2$)	1.00	1.00	1.00	1.00
$1.1 \le g \le 2.2$	1.00 ± 0.01 (+0%)	1.01 ± 0.01 (+1%)	1.01 ± 0.02 (+1%)	1.03 ± 0.02 (+3%)
$1.25 \le g \le 2.2$	1.00 ± 0.01 (+0%)	1.03 ± 0.02 (+3%)	1.05 ± 0.03 (+5%)	1.11 ± 0.05 (+11%)
$1.4 \le g \le 2.2$	1.04 ± 0.02 (+4%)	1.19 ± 0.07 (+19%)	1.30 ± 0.12 (+30%)	1.46 ± 0.16 (+46%)

[a]Updraft velocity.
[b]Number concentrations of CCN.
[c]Number concentrations of cloud droplets.
[d]Effective radius of cloud droplets.

small changes indicated that N_{CCN}, N_{cd}, and R_{eff} were reasonably estimated from the distributions of g and the number-size distributions from the HTDMA and SMPS, even without the CCNC data. However, the corrections explained above were included in the model to seek higher reliability in the estimates for this study.

3.6. Contribution of Aerosol Particles With Different Hygroscopicity to Cloud Droplet Formation and Growth

In this section, we assess the contribution of particles grouped by hygroscopicity to the number concentrations and properties of cloud droplets. The primary objective of this sensitivity study was to investigate the importance of less hygroscopic particles, which were abundant in the urban aerosol, for cloud droplet formation in the urban atmosphere. This was performed by investigating the changes in N_{CCN}, N_{cd}, and R_{eff} by considering the presence of less hygroscopic particles in addition to more hygroscopic particles ($0.8 \le g \le 2.2$), as compared to the hypothetical cases that only more hygroscopic particles ($g \ge 1.25$) were present. If urban aerosols are taken as an analogy, the latter case corresponds to aerosols entering the urban area after long-range transport, and the former corresponds to aerosols after less hygroscopic particles are added to these aerosols over the urban area [*Zaveri et al.*, 2010].

Figures 10a–10c show the mean values of N_{CCN}, N_{cd}, and R_{eff} in the cases of particles in the ranges of $0.8 \le g \le 2.2$ (i.e., all particles are present), and $1.25 \le g \le 2.2$ (only more hygroscopic particles are present). The results in the other cases that particles in the ranges of $1.1 \le g \le 2.2$ and $1.4 \le g \le 2.2$ were considered are also shown in Figure 10. Figures 10d–10f show the ratios of N_{CCN}, N_{cd}, and R_{eff} in each case to those variables over the entire range of $0.8 \le g \le 2.2$ ($N_{CCN,all}$, $N_{cd,all}$, and $R_{eff,all}$). The mean values in the four cases are summarized in Table 3. As seen in Figure 10 and Table 3, N_{CCN}, N_{cd}, and R_{eff} depended largely on v. If v was high (1.0 and 5.0 m s^{-1}), N_{cd} increased and R_{eff} decreased markedly considering the particle had a wider range of g in the model. In the base case that all particles with $0.8 \le g \le 2.2$ were included at v of 1.0 m s^{-1} (or 5.0 m s^{-1}), N_{cd} was 18% (36%) larger and R_{eff} was 5% (10%) smaller on average, as compared to the case that only more hygroscopic particles were present. N_{CCN} was also larger on average by 27% (43%). In contrast, if v was very

low (0.1 m s^{-1}), N_{CCN}, N_{cd}, and R_{eff} did not show differences regardless of the model cases. The ratio of $N_{cd}/N_{cd,all}$ was about 1 except for the case when only particles with g larger than 1.4 were considered (Figure 10e). This suggested that most of the particles that could be activated as cloud droplets were highly hygroscopic ($g \geq 1.4$) at low v and low SS. From this, it was apparent that the presence/absence of less hygroscopic particles was not important for the formation of cloud droplets under extremely low v.

The results in Figure 10 and Table 3 show that the presence of less hygroscopic particles contributed substantially to N_{CCN} and N_{cd} and led to smaller cloud droplets except in the case of small v. *Facchini et al*. [1999] reported that a 20% increase of N_{CCN} led to 1% enhancement of local top-of-atmosphere albedo and a decrease of -1 W m^{-2} radiative forcing in the case of the formation of stratus clouds (SS of ~0.5%). In this study, the presence of less hygroscopic particles contributed to a 27% increase of N_{CCN} with v of 1.0 m s^{-1} at S_{max} of ~0.47% (Figure 10d), which may corresponded to a decrease in the local radiative forcing on the order of 1 W m^{-2}.

Results from the cloud parcel model in this study showed that the hygroscopicity of aerosol particles has a large influence on the CCN and cloud droplet activation, as suggested from recent studies [*Anttila et al*., 2009; *Liu and Wang*, 2010]. The varying importance of less hygroscopic particles to cloud droplet formation depending on v illustrated the importance of information about the hygroscopicity as well as size distribution. Our results demonstrated that HTDMA-derived two-dimensional particle number distributions versus g and $d_{p,dry}$ are useful to analyze the cloud droplet activation based on it. For this purpose, the CCNC data may not be necessary because there was little bias from the differences of $d_{act,g85}$ from $d_{act,CCN}$ (i.e., surface tension and solute effect) and F_{max} values less than unity (i.e., presence of inactive particles). However, these variables have important implications for the properties and processing of less hygroscopic particles, for example, the degree of change in hygroscopicity of less hygroscopic particles by aging in the atmosphere. The outcome of this study is based on the analysis of the data from a short observation period at a single site. Moreover, the temporal variations of aerosols in the studied area may not be fully captured because of the low time resolution of data. Further investigation (i.e., comparison with results from other locations and seasons and with those based on experiments in longer periods) may generalize our conclusion or may bring new findings about the variability, depending on atmospheric environments.

4. Summary

The number-size distributions, the distributions of g at 85% RH, and the ratios of CCN to CN for particles with g_{set} of 1.0, 1.1, 1.25, and 1.4 at 16 dry mobility diameters ($d_{p,dry}$) were obtained from atmospheric aerosols over the city of Nagoya, Japan. The observed particles were present abundantly in the Aitken mode range. The distribution of g had on average less and more hygroscopic modes. In the lowest hygroscopicity range ($0.8 \leq g < 1.1$), the number concentrations of particles had a maximum in the Aitken mode range and decreased toward the accumulation mode range. In contrast, in the highest hygroscopicity range ($1.4 \leq g \leq 2.2$), the number concentrations of particles in the accumulation mode range were substantially higher as compared to those in the Aitken mode range. The CCN efficiency spectra of more hygroscopic particles with g_{set} of 1.25 and 1.4 were characterized by a sharp increase in $n_{DMA2,CCN}/n_{DMA2,CN}$, small $\sigma_{CCN}/d_{act,CCN}$, and large F_{max} values. Obtained results lead to the conclusion showed that the hygroscopicity of more hygroscopic particles at 85% RH was well linked to the CCN activity. In contrast, CCN efficiency spectra of less hygroscopic particles with g_{set} of 1.0 and 1.1 were characterized by a moderate increase in $n_{DMA2,CCN}/n_{DMA2}$, large $\sigma_{CCN}/d_{act,CCN}$, and small F_{max} values. Results showed that some of the less hygroscopic particles remained CCN-inactive even in the case of high SS and large diameters.

To investigate the relation between the hygroscopic growth and the CCN activation, CCN activation diameters predicted from the g distributions ($d_{act,g85}$) were compared with measured ($d_{act,CCN}$) for aerosol particles with different g_{set}. The $d_{act,CCN}$ were smaller than $d_{act,g85}$ with one exception, that is, the measured CCN activity was higher than predicted. Although the differences of $d_{act,g85}$ from $d_{act,CCN}$ were on average within 12% for more hygroscopic particles, the differences were on average larger (16%–41%) for less hygroscopic particles. The possible causes for this difference included the surface tension reduction due to organics or surface-active compounds, the dependence of κ on the concentration of the aqueous solution, the existence of sparingly soluble particles, and asphericity of particles.

In the cloud parcel model used to estimate N_{CCN}, N_{cd}, and R_{eff}, the differences of $d_{act,g85}$ from $d_{act,CCN}$ and the existence of CCN-inactive particles were found to have a small influence on cloud droplet formation. The

contribution of aerosol particles with different hygroscopicity to cloud droplet formation was investigated using the model. The presence of less hygroscopic particles in addition to more hygroscopic particles ($0.8 \le g \le 2.2$) led to 27% (43%) increase of N_{CCN}, 18% (36%) increase of N_{cd}, and the 5% (10%) decrease of R_{eff} at v of 1.0 m s^{-1} (or 5.0 m s^{-1}) as compared to the case that only more hygroscopic particles ($g \ge 1.25$) were present. These results suggested that the presence of less hygroscopic particles can contribute substantially to N_{CCN} and N_{cd} and can lead to smaller cloud droplets. This study demonstrated that HTDMA-derived distributions of aerosol hygroscopicity are useful for the prediction of cloud droplet activation. Our results suggest that, for this purpose, the CCNC data may not necessarily be required for reliable estimations.

Appendix A

A1. Influences of Multiply Charged Particles on Data of Hygroscopic Growth and CCN Activation

The particles selected in DMA1 of the HTDMA include multiply charged particles in addition to singly charged particles. The presence of multiply charged particles engenders some biases of the measured data [*Duplissy et al*., 2009; *Gysel et al*., 2009] because the changes in the electrical mobility of particles by the hygroscopic growth depend on the dry diameters, which differ for particles with same electrical mobility but with different numbers of charges. Moreover, the differences of g distributions of singly and multiply charged particles bias the g distributions obtained on the assumption that all particles with charges are singly charged. In this study, we regard these biases as acceptable, as explained below. The former of the biases was assessed by calculating the differences of g of multiply charged particles from that of singly charged particles having the same mobility diameter. The biases of g of doubly and triply charged particles are presented respectively in Figures S5a and S5b. As the figures show, the biases of g for doubly and triply charged particles in the range of $0.8 \le g \le 2.2$ are within 9% and 13%, respectively. The biases of particles with g of 1.0, 1.1, 1.25, and 1.4 for doubly and triply charged particles are within 6% and 7%, respectively. Figures S6a–S6d present the number fractions of singly, doubly, and triply charged particles in the four ranges of g. In the range of $0.8 \le g < 1.4$, the fraction of singly charged particles is more than 80% in most of the cases of the averages at each $d_{p,dry}$. In the range of $1.4 \le g \le 2.2$, the fraction of singly charged particles is more than 60% in all but one of the cases of the averages at each $d_{p,dry}$. If the biases of $d_{act,gset}$ and $d_{act,g85}$ are assumed to be given by the products of the number fraction of multiply charged (i.e., either doubly or triply) particles and their biases of g, then the biases of $d_{act,gset}$ and $d_{act,g85}$ with 20% multiply charged (i.e., doubly or triply) particles are within 1% for particles with g_{set} of 1.0, 1.1, and 1.25. The biases of $d_{act,gset}$ and $d_{act,g85}$ with 40% multiply charged (i.e., doubly or triply) particles are within 3% for particles with g_{set} of 1.4. Comparison of this result to that in Figure 8 shows that the biases attributable to the differences of g of multiply charged particles are not remarkable. The latter of the two biases, which results from the differences of g distributions of singly charged particles and those of multiply charged particles are evaluated using the following equation.

$$\left[\left.\frac{dN}{d\log d_{p,dry}}\right|_{d_{p,dry}=d_1} \cdot I(dj) f(d_1,1) + \left.\frac{dN}{d\log d_{p,dry}}\right|_{d_{p,dry}=d_2} \cdot I(dj) f(d_2,2) + \left.\frac{dN}{d\log d_{p,dry}}\right|_{d_{p,dry}=d_3} \cdot I(dj) f(d_3,3)\right] p_{apparent}(d_1,i)$$
$$\cong \left.\frac{dN}{d\log d_{p,dry}}\right|_{d_{p,dry}=d_1} \cdot I(dj) f(d_1,1) p_{true}(d_1,i) + \left.\frac{dN}{d\log d_{p,dry}}\right|_{d_{p,dry}=d_2} \cdot I(dj) f(d_2,2) p_{true}(d_2,i)$$
$$+ \left.\frac{dN}{d\log d_{p,dry}}\right|_{d_{p,dry}=d_3} \cdot I(dj) f(d_3,3) p_{true}(d_3,i) \quad \text{(A1)}$$

Here, d_j denotes the dry mobility diameters of $+j$ charged particles ($j = 1, 2, 3$) selected in DMA1. The $dN/d\log d_{p,dry}$ represents the number-size distribution of aerosol particles in the atmosphere and I (d_j) is the factor to correct for diffusion losses in the sampling line [*Mochida et al*., 2010]. The f (d_j, j) are the number fractions of $+j$ charged particles ($j = 1, 2, 3$) [*Wiedensohler*, 1988; *TSI Incorporated*, 2006]. The $p_{apparent}$ (d_j, i) and p_{true} (d_j, i) respectively stand for the apparent (i.e., biased by the presence of multiply charged particles) and true probabilities of the presence of particles in the four ranges of g (numbered using i). In this calculation, the biases of g in Figure S5 were not considered. We regard it as reasonable because the biases are not large as compared to the ranges of g. The presence of doubly and triply particles above 359 nm was not considered

because of the absence of g distribution data. The d_j in $f(d_j, j)$ was replaced by the values in the nearest setting diameters used for size selection in DMA1. In addition, and $p_{true}(d_2, i)$ and $p_{true}(d_3, i)$ are approximated by $p_{apparent}(d_2, i)$ and $p_{apparent}(d_3, i)$ in equation (A1), respectively, with replacement of d_j by the nearest setting diameters of DMA1. The calculated biases of g distributions by the presence of doubly and triply charged particles, $\{[p_{apparent}(d_1, i)/p_{true}(d_1, i)] - 1\}$ (Figure S7) at each dry diameter from 24.1 to 359 nm are on average within the range from −3% to 24%. We regard that the biases of g distributions by the presence of multiply charged particles are not large and the biases are acceptable for the analysis of cloud droplet formation in sections 3.5 and 3.6. The modest biases indicate that the above described approximation of the true probabilities by the apparent probabilities is self consistent.

The presence of multiply charged particles also biases CCN-effective spectra from CCNC and CPC data because CCN activity of multiply charged particles tends to be higher than that of singly charged particles with the same electrical mobility. For the analysis of this study, we calculated the CCN-effective spectra for singly charged particles as follows. The fractions of multiply charged particles with specific $d_{p,dry}$ downstream of DMA2 are estimated from the SMPS-derived number-size distributions on the assumption that the fraction of multiply charged particles selected in DMA1 did not change by the further selection in DMA2. This assumption is consistent with the result that the differences of g of multiply charged particles from singly charged particles having the same mobility diameter (Figures S5a and S5b) are not large. The $n_{CCN,DMA2}/n_{CN,DMA2}$ at each $d_{p,dry}$ was obtained by calculating the number fractions of doubly and triply charged particles based on the theoretical formulas [*Wiedensohler*, 1988; *TSI Incorporated*, 2006], and by subtracting the contribution of doubly and triply charged particles as CCN preferentially from raw $n_{CCN,DMA2}$ on the assumption that CCN activity of multiply charged particles is higher than that of singly charged particles. The contributions of doubly and triply charged particles were calculated based on 3 h average number-size distributions of aerosol particles in the atmosphere with considerations of the diffusion losses in the sampling line and the areas of the transfer functions of DMA1 [*Mochida et al.*, 2010].

This assumption is not entirely correct because all multiply charged particles are not necessarily CCN active as suggested from F_{max} less than unity. To evaluate the validity of the method explained above, we examined a method to correct $n_{CCN,DMA2}/n_{CN,DMA2}$ by considering $n_{CCN,DMA2}/n_{CN,DMA2}$ of doubly and triply charged particles sequentially from large to small diameters (Figure S8). Here, the presence of doubly and triply particles above 359 nm in $n_{CCN,DMA2}$ were not considered because of the absence of data. In this method, the differences of the CCN activation diameters predicted based on g ($d_{act,g85}$) from those measured ($d_{act,CCN}$) were within 17% and 18–46%, respectively, for more and less hygroscopic particles. These values are similar to the corresponding values in section 3.3 (12% and 16–41%, respectively). Furthermore, the feature that $d_{act,CCN}$ tends to be smaller than $d_{act,g85}$ holds, although the number of the exceptional cases that $d_{act,CCN}$ is larger than $d_{act,g85}$ increases to three from one. The results obtained from this method were not used for this study because some CCN efficiency spectra seem to be unrealistically scattered (Figure S8). This scattering might be associated in part with the uncertainties of $n_{CCN,DMA2}/n_{CN,DMA2}$ of multiply charged particles as a result of the temporal variation of CCN number concentrations during the dry diameter scans conducted using DMA1.

A2. Uncertainty in the Model Calculation

As described in section 2.3, a single κ value was applied to all particles in the model calculation. To assess the possible influence of this simplification, we changed the κ value in the model from 0.61 to 0.017 (the mean κ of aerosol particles with g_{set} of 1.0) and 0.18 (the mean κ of aerosol particles of 16 $d_{p,dry}$ for the 11 time periods) by converting particle diameters without changing S_{crit} for each particle. If κ was assumed to be 0.017 (or 0.18) at v of 0.1–5.0 m s^{-1}, N_{cd} and R_{eff} agreed with the results in the base case within 12% and 5% (or 6% and 3%), respectively. This agreement indicated that the influence due to the dependence of κ was small for the purpose of this study. We therefore concluded that a single κ can be used for the assessment of aerosols in which particles with different hygroscopicity are mixed as observed in Nagoya. It should be emphasized that the most appropriate κ for the particles is not obvious; it would be the mean κ of all particle components or the mean κ of the soluble fractions, which may depend on the particle morphology that governs the initial hygroscopic growth of the particles.

Uncertainty associated with the extrapolation of the number-size distributions of aerosol particles to >359 nm was presumably small. Even if the number concentrations of particles >359 nm were forced to be zero, the changes in N_{cd} and R_{eff} from the base case were within 1% for each.

Acknowledgments
We thank C. Nishita-Hara for her contribution to the preliminary study for this paper. We also thank K. Osada for providing a DMA. We acknowledge the National Oceanic and Atmospheric Administration (NOAA) Air Resources Laboratory (ARL) for the use of the Hybrid Single-Particle Lagrangian Integrated Trajectory (HYSPLIT) model. This study was supported partly by a Grant-in-Aid for Young Scientists (S) (20671001). The data used for this paper are available on request to the corresponding author.

References

Abbatt, J. P. D., K. Broekhuizen, and P. P. Kumar (2005), Cloud condensation nucleus activity of internally mixed ammonium sulfate/organic acid aerosol particles, *Atmos. Environ.*, *39*, 4767–4778, doi:10.1016/j.atmosenv.2005.04.029.

Aikawa, M., T. Ohara, T. Hiraki, O. Oishi, A. Tsuji, M. Yamagami, K. Murano, and H. Mukai (2010), Significant geographic gradients in particulate sulfate over Japan determined from multiple-site measurements and a chemical transport model: Impacts of transboundary pollution from the Asian continent, *Atmos. Environ.*, *44*, 381–391, doi:10.1016/j.atmosenv.2009.10.025.

Albrecht, B. A. (1989), Aerosols cloud microphysics, and fractional cloudiness, *Science*, *245*, 1227–1230, doi:10.1126/science.245.4923.1227.

Anttila, T., P. Vaattovaara, M. Komppula, A.-P. Hyvärinen, H. Lihavainen, V.-M. Kerminen, and A. Laaksonen (2009), Size-dependent activation of aerosols into cloud droplets at a subarctic background site during the second Pallas Cloud Experiment (2nd PaCE): Method development and data evaluation, *Atmos. Chem. Phys.*, *9*, 4841–4854, doi:10.5194/acp-9-4841-2009.

Bilde, M., and B. Svenningsson (2004), CCN activation of slightly soluble organics: The importance of small amounts of inorganic salt and particle phase, *Tellus*, *56B*, 128–134.

Broekhuizen, K., P. P. Kumar, and J. P. D. Abbatt (2004), Partially soluble organics as cloud condensation nuclei: Role of trace soluble and surface active species, *Geophys. Res. Lett.*, *31*, D01107, doi:10.1029/2003GL018203.

Chuang, P. Y. (2003), Measurement of the timescale of hygroscopic growth for atmospheric aerosols, *J. Geophys. Res.*, *108*(D9), 4282, doi:10.1029/2002JD002757.

Clegg, S. L., P. Brimblecombe, and A. S. Wexler (1998), A thermodynamic model of the system $H^+ - NH_4^+ - SO_4^{2-} - NO_3^- - H_2O$ at tropospheric temperatures, *J. Phys. Chem. A*, *102*, 2137–2154.

Cubison, M. J., B. Ervens, G. Feingold, K. S. Docherty, I. M. Ulbrich, L. Shields, K. Prather, S. Hering, and J. L. Jimenez (2008), The influence of chemical composition and mixing state of Los Angeles urban aerosol on CCN number and cloud properties, *Atmos. Chem. Phys.*, *8*, 5649–5667, doi:10.5194/acp-8-5649-2008.

Duplissy, J., et al. (2008), Cloud forming potential of secondary organic aerosol under near atmospheric conditions, *Geophys. Res. Lett.*, *35*, D03818, doi:10.1029/2007GL031075.

Duplissy, J., et al. (2009), Intercomparison study of six HTDMAs: Results and recommendations, *Atmos. Meas. Tech.*, *2*, 363–378.

Ervens, B., G. Feingold, G. J. Frost, and S. M. Kreidenweis (2004a), A modeling study of aqueous production of dicarboxylic acids: 1. Chemical pathways and speciated organic mass production, *J. Geophys. Res.*, *109*, D15205, doi:10.1029/2003JD004387.

Ervens, B., G. Feingold, S. L. Clegg, and S. M. Kreidenweis (2004b), A modeling study of aqueous production of dicarboxylic acids: 2. Implications for cloud microphysics, *J. Geophys. Res.*, *109*, D15206, doi:10.1029/2004JD004575.

Facchini, M. C., M. Mircea, S. Fuzzi, and R. J. Charlson (1999), Cloud albedo enhancement by surface-active organic solutes in growing droplets, *Nature*, *401*, 257–259, doi:10.1038/45758.

Facchini, M. C., S. Decesari, M. Mircea, S. Fuzzi, and G. Loglio (2000), Surface tension of atmospheric wet aerosol and cloud/fog droplets in relation to their organic carbon content and chemical composition, *Atmos. Environ.*, *34*, 4853–4857.

Fors, E. O., E. Swietlicki, B. Svenningsson, A. Kristensson, G. P. Frank, and M. Sporre (2011), Hygroscopic properties of the ambient aerosol in southern Sweden—A two year study, *Atmos. Chem. Phys.*, *11*, 8343–8361, doi:10.5194/acp-11-8343-2011.

Fountoukis, C., et al. (2007), Aerosol–cloud drop concentration closure for clouds sampled during the International Consortium for Atmospheric Research on Transport and Transformation 2004 campaign, *J. Geophys. Res.*, *112*, D10S30, doi:10.1029/2006JD007272.

Gasparini, R., D. R. Collins, E. Andrews, P. J. Sheridan, J. A. Ogren, and J. G. Hudson (2006), Coupling aerosol size distributions and size-resolved hygroscopicity to predict humidity-dependent optical properties and cloud condensation nuclei spectra, *J. Geophys. Res.*, *111*, D05S13, doi:10.1029/2005JD006092.

Good, N., et al. (2010), Widening the gap between measurement and modelling of secondary organic aerosol properties?, *Atmos. Chem. Phys.*, *10*, 2577–2593, doi:10.5194/acp-10-2577-2010.

Gysel, M., G. B. McFiggans, and H. Coe (2009), Inversion of tandem differential mobility analyser (TDMA) measurements, *Aerosol Sci.*, *40*, 134–151, doi:10.1016/j.jaerosci.2008.07.013.

Henning, S., T. Rosenørn, B. D'Anna, A. A. Gola, B. Svenningsson, and M. Bilde (2005), Cloud droplet activation and surface tension of mixtures of slightly soluble organics and inorganic salt, *Atmos. Chem. Phys.*, *5*, 575–582, doi:10.5194/acp-5-575-2005.

Intergovernmental Panel on Climate Change (2007), *Climate Change 2007: The Physical Science Basis, Fourth Assessment Report of the Intergovernmental Panel on Climate Change*, edited by S. Solomon et al., Cambridge Univ. Press, Cambridge and New York.

Kreidenweis, S. M., M. D. Petters, and P. J. DeMott (2008), Single-parameter estimates of aerosol water content, *Environ. Res. Lett.*, *3*(2008), 035002, doi:10.1088/1748-9326/3/3/035002.

Kuba, N., and T. Takeda (1983), Numerical study of the effect of CCN on the size distribution of cloud droplets. Part II: Formation of large droplets, *J. Meteorol. Soc. Jpn.*, *61*, 375–387.

Kuba, N., H. Iwabuchi, K. Maruyama, T. Hayasaka, T. Takeda, and Y. Fujiyoshi (2003), Parameterization of the effect of cloud condensation nuclei on optical properties of a non-precipitating water layer cloud, *J. Meteorol. Soc. Jpn.*, *81*(2), 393–414.

Kuwata, M., and Y. Kondo (2008), Dependence of size-resolved CCN spectra on the mixing state of nonvolatile cores observed in Tokyo, *J. Geophys. Res.*, *113*, D19202, doi:10.1029/2007JD009761.

Lance, S., A. Nenes, and T. A. Rissman (2004), Chemical and dynamical effects on cloud droplet number: Implications for estimates of the aerosol indirect effect, *J. Geophys. Res.*, *109*, D22208, doi:10.1029/2004JD004596.

Leaitch, W. R., et al. (2010), Cloud albedo increase from carbonaceous aerosol, *Atmos. Chem. Phys.*, *10*, 7669–7684, doi:10.5194/acp-10-7669-2010.

Liu, X., and J. Wang (2010), How important is organic aerosol hygroscopicity to aerosol indirect forcing?, *Environ. Res. Lett.*, *5*(2010), 044010, doi:10.1088/1748-9326/5/4/044010.

Menon, S., J. Hansen, L. Nazarenko, and Y. Luo (2002), Climate effects of black carbon aerosols in China and India, *Science*, *297*, 2250–2253.

Mochida, M., T. Miyakawa, N. Takegawa, Y. Morino, K. Kawamura, and Y. Kondo (2008), Significant alteration in the hygroscopic properties of urban aerosol particles by the secondary formation of organics, *Geophys. Res. Lett.*, *35*, L02804, doi:10.1029/2007GL031310.

Mochida, M., C. Nishita-Hara, Y. Kitamori, S. G. Aggarwal, K. Kawamura, K. Miura, and A. Takami (2010), Size-segregated measurements of cloud condensation nucleus activity and hygroscopic growth for aerosols at Cape Hedo, Japan, in spring 2008, *J. Geophys. Res.*, *115*, D21207, doi:10.1029/2009JD013216.

Mochida, M., C. Nishita-Hara, H. Furutani, Y. Miyazaki, J. Jung, K. Kawamura, and M. Uematsu (2011), Hygroscopicity and cloud condensation nucleus activity of marine aerosol particles over the western North Pacific, *J. Geophys. Res.*, *116*, D06204, doi:10.1029/2010JD014759.

Nenes, A., S. Ghan, H. Abdul-Razzak, P. Y. Chuang, and J. H. Seinfeld (2001), Kinetic limitations on cloud droplet formation and impact on cloud albedo, *Tellus*, *53B*, 133–149.

Padró, L. T., D. Tkacik, T. Lathem, C. J. Hennigan, A. P. Sullivan, R. J. Weber, L. G. Huey, and A. Nenes (2010), Investigation of cloud condensation nuclei properties and droplet growth kinetics of the water-soluble aerosol fraction in Mexico City, *J. Geophys. Res.*, *115*, D09204, doi:10.1029/2009JD013915.

Petters, M. D., and S. M. Kreidenweis (2007), A single parameter representation of hygroscopic growth and cloud condensation nucleus activity, *Atmos. Chem. Phys.*, *7*, 1961−1971, doi:10.5194/acp-7-1961-2007.

Prenni, A. J., M. D. Petters, S. M. Kreidenweis, P. J. DeMott, and P. J. Ziemann (2007), Cloud droplet activation of secondary organic aerosol, *J. Geophys. Res.*, *112*, D10223, doi:10.1029/2006JD007963.

Rissler, J., E. Swietlicki, J. Zhou, G. Roberts, M. O. Andreae, L. V. Gatti, and P. Artaxo (2004), Physical properties of the sub-micrometer aerosol over the Amazon rain forest during the wet-to-dry season transition-comparison of modeled and measured CCN concentrations, *Atmos. Chem. Phys.*, *4*, 2119−2143, doi:10.5194/acp-4-2119-2004.

Rose, D., S. S. Gunthe, E. Mikhailov, G. P. Frank, U. Dusek, M. O. Andreae, and U. Pöschl (2008), Calibration and measurement uncertainties of a continuous-flow cloud condensation nuclei counter(DMT-CCNC): CCN activation of ammonium sulfate and sodium chloride aerosol particles in theory and experiment, *Atmos. Chem. Phys.*, *8*, 1153−1179, doi:10.5194/acp-8-1153-2008.

Rose, D., A. Nowak, P. Achtert, A. Wiedensohler, M. Hu, M. Shao, Y. Zhang, M. O. Andreae, and U. Pöschl (2010), Cloud condensation nuclei in polluted air and biomass burning smoke near the mega-city Guangzhou, China—Part 1: Size-resolved measurements and implications for the modeling of aerosol particle hygroscopicity and CCN activity, *Atmos. Chem. Phys.*, *10*, 3365–3383, doi:10.5194/acp-10-3365-2010.

Rosenfeld, D. (1999), TRMM observed first direct evidence of smoke from forest fires inhibiting rainfall, *Geophys. Res. Lett.*, *26*(20), 3105−3108.

Rosenfeld, D. (2000), Suppression of rain and snow by urban and industrial air pollution, *Science*, *287*, 1793−1796.

Reutter, P., H. Su, J. Trentmann, M. Simmel, D. Rose, S. S. Gunthe, H. Wernli, M. O. Andreae, and U. Pöschl (2009), Aerosol- and updraft-limited regimes of cloud droplet formation: Influence of particles number, size and hygroscopicity on the activation of cloud condensation nuclei (CCN), *Atmos. Chem. Phys.*, *9*, 7067−7080, doi:10.5194/acp-9-7067-2009.

Shantz, N. C., W. R. Leaitch, and P. F. Caffrey (2003), Effect of organics of low solubility on the growth rate of cloud droplets, *J. Geophys. Res.*, *108*(D5), 4168, doi:10.1029/2002JD002540.

Shulman M. L., M. C. Jacobson, R. J. Carlson, R. E. Synovec, and T. E. Young (1996), Dissolution behavior and surface tension effects of organic compounds in nucleating cloud droplets, *Geophys. Res. Lett.*, *23*(3), 277−280.

Sjogren, S., M. Gysel, E. Weingartner, U. Baltensperger, M. J. Cubison, H. Coe, A. A. Zardini, C. Marcolli, U. K. Krieger, and T. Peter (2007), Hygroscopic growth and water uptake kinetics of two-phase aerosol particles consisting of ammonium sulfate, adipic and humic acid mixtures, *Aerosol Sci.*, *38*, 157−171, doi:10.1016/j.jaerosci.2006.11.005.

Takeda, T., and N. Kuba (1982), Numerical study of the effect of CCN on the size distribution of cloud droplets. Part I: Cloud droplets in the stage of condensation growth, *J. Meteorol. Soc. Jpn.*, *60*, 978−993.

Takemura, T., T. Nozawa, S. Emori, T. Y. Nakajima, and T. Nakajima (2005), Simulation of climate response to aerosol direct and indirect effects with aerosol transport-radiation model, *J. Geophys. Res.*, *110*, D02202, doi:10.1029/2004JD005029.

Tang, I. N., and H. R. Munkelwitz (1994), Water activities, densities, and refractive indices of aqueous sulfates and sodium nitrate droplets of atmospheric importance, *J. Geophys. Res.*, *99*(D9), 18,801−18,808.

Tritscher, T., et al. (2011), Changes of hygroscopicity and morphology during ageing of diesel soot, *Environ. Res. Lett.*, *6*(2011), 034026, doi:10.1088/1748-9326/6/3/034026.

TSI Incorporated (2006), Model 3936 scanning mobility particles sizer™ (SMPS™) spectrometer, operation and service manual, *P/N 1933796*, Revision L. Shoreview, Minn.

Twomey, S. A. (1977), The influence of pollution on the shortwave albedo of clouds, *J. Atmos. Sci.*, *34*, 1149−1152.

Vestin, A., J. Rissler, E. Swietlicki, G. P. Frank, and M. O. Andreae (2007), Cloud-nucleating properties of the Amazonian biomass burning aerosol: Cloud condensation nuclei measurements and modeling, *J. Geophys. Res.*, *112*, D14201, doi:10.1029/2006JD008104.

Wang, J., M. J. Cubison, A. C. Aiken, J. L. Jimenez, and D. R. Collins (2010), The importance of aerosol mixing state and size-resolved composition on CCN concentration and the variation of the importance with atmospheric aging of aerosols, *Atmos. Chem. Phys.*, *10*, 7267−7283, doi:10.5194/acp-10-7267-2010.

Wex, H., F. Stratmann, D. Topping, and G. McFiggans (2008), The Kelvin versus the Raoult term in the Köhler equation, *J. Aerosol Sci.*, *65*, 4004−4016, doi:10.1175/2008JAS2720.1

Wex, H., M. D. Petters, C. M. Carrico, E. Hallbauer, A. Massling, G. R. McMeeking, L. Poulain, Z. Wu, S. M. Kreidenweis, and F. Stratmann (2009), Towards closing the gap between hygroscopic growth and activation for secondary organic aerosol: Part I—Evidence from measurements, *Atmos. Chem. Phys.*, *9*, 3987−3997, doi:10.5194/acp-9-3987-2009.

Wiedensohler, A. (1988), Technical Note: An approximation of the bipolar charge distribution for particles in the submicron size range, *J. Aerosol Sci.*, *19*, 387−389.

Wonaschuetz, A., A. Sorooshian, B. Ervens, P. Y. Chuang, G. Feingold, S. M. Murphy, J. de Gouw, C. Warneke, and H. H. Jonsson (2012), Aerosol and gas re-distribution by shallow cumulus clouds: An investigation using airborne measurements, *J. Geophys. Res.*, *117*, D17202, doi:10.1029/2012JD018089.

Yoshitomi, M., O. Wild, and H. Akimoto (2011), Contributions of regional and intercontinental transport to surface ozone in the Tokyo area, *Atmos. Chem. Phys.*, *11*, 7583−7599, doi:10.5194/acp-11-7583-2011.

Zaveri, R. A., J. C. Barnard, R. C. Easter, N. Riemer, and M. West (2010), Particle-resolved simulation of aerosol size, composition, mixing state, and the associated optical and cloud condensation nuclei activation properties in an evolving urban plume, *J. Geophys. Res.*, *115*, D17210, doi:10.1029/2009JD013616.

Zhang, Q., M. R. Canagaratna, J. T. Jayne, D. R. Worsnop, and J.-L. Jimenez (2005a), Time- and size-resolved chemical composition of submicron particles in Pittsburgh: Implications for aerosol sources and processes, *J. Geophys. Res.*, *110*, D07S09, doi:10.1029/2004JD004649.

Zhang, Q., D. R. Worsnop, M. R. Canagaratna, and J.-L. Jimenez (2005b), Hydrocarbon-like and oxygenated organic aerosols in Pittsburgh: Insights into sources and processes of organic aerosols, *Atmos. Chem. Phys.*, *5*, 3289−3311, doi:10.5194/acp-5-3289-2005.